Delft University of Technology

The steering and course keeping qualities of high-speed craft and the inception of dynamic instabilities in the following sea

Bonci, M.; De Jong, P.; Van Walree, F.; Renilson, M. R.; Huijsmans, R. H.M.

Important note
To cite this publication, please use the final published version (if applicable).
Please check the document version above.

The steering and course keeping qualities of high-speed craft and the inception of dynamic instabilities in the following sea

M. Bonci [a],[*], P. De Jong [b], F. Van Walree [b], M.R. Renilson [c], R.H.M. Huijsmans [d]

[a] *Delft University of Technology, Mekelweg 2, 2628, CD Delft, the Netherlands*
[b] *MARIN, Wageningen, the Netherlands*
[c] *Australian Maritime College, University of Tasmania, Australia*
[d] *Delft University of Technology, the Netherlands*

ABSTRACT

Small high-speed craft are the most vulnerable to the severity of the sea: achieving a design which pairs good performance and acceptable levels of safety is not a trivial task. The seakeeping and manoeuvrability of these vessels play a crucial role in following sea conditions: dynamic instabilities, namely broaching-to and surf-riding, are more than a rare eventuality and threaten the survivability of the vessel and the life of the mariners. This study investigates the effects of the steering qualities on the broaching-to behaviour of a high-speed craft when it is sailing in following and stern-quartering waves.

The motions and loads of the vessel are simulated by means of a 3D time domain blended potential flow boundary element method (BEM), validated using captive model tests in regular waves carried out at the Seakeeping and Manoeuvring Basin (SMB) of MARIN. The hull directional stability and turning ability of the high-speed craft were artificially modified, showing that an increase in the directional stability as well as in the effectiveness of the steering can be beneficial to avoid the inception of broaching-to, but they have different consequences on the dynamics of the vessel's loss of control.

1. Introduction

The first research studies on the controllability of ships focused on displacement merchant vessels manoeuvring in calm water. The most important aspects of the manoeuvrability of such ships were related to their ability to maintain a straight course with the minimum steering effort, and to stop quickly before an obstacle or to avoid it by a safe turn, for example. These principles are still valid nowadays (Resolution, 2002), and ships are designed according to these safety requirements.

The studies on the manoeuvrability of displacement vessels are numerous. The same cannot be said for high-speed craft. Usually high-speed vessels must possess very good steering capabilities in order to be very manoeuvrable, but they must also be able to easily maintain their course in a seaway. From a technical point of view, the controllability of small hard-chine fast craft is more complicated because it depends on several factors which are not usually considered for conventional displacement ships: forward speed, vertical running attitude, wave making effects and flow separation on knuckles are decisive factors in the manoeuvring behaviour of small fast vessels.

The manoeuvring characteristics of high-speed craft can be very important in rough seas. Small vessels are more subjected than big displacement ships to dangerous motions and large fluctuations of forward speed. The hazard related to small vessels sailing in the following sea is well-known. Dynamic instability phenomena such as broaching-to are events strongly dreaded by mariners. A broach, or broaching-to, is the involuntary yawing movement of the vessel caused by the incoming following wave; the vessel suddenly turns broadside to the seaway because of the large destabilizing wave yawing moment. In this situation the steering is difficult and the vessel continues a turning motion despite the maximum control counter-action from the rudder. The loss of control of the ship puts the safety of the crew on board in great danger. In extreme cases, broaching-to can lead to the capsize of the vessel.

The characteristics of the phenomenon of broaching-to are well known (Du Cane and Goodrich, 1962; Spyrou, 1996; Umeda, 1999; Umeda and Matsuda, 2000; Renilson, 1981, 2014; Renilson and Driscoll, 1982). According to the definition by Cohen and Blount (1986), broaching-to is a non-oscillatory combined yaw-roll dynamic instability which occurs at medium-high speed, typically at a length Froude

number higher than *0.3*. The ships which are more subjected to such dynamic instability are therefore relatively small vessels (up to *70* m in length) which operate in the pre-planing regime: high-speed craft, fishing vessels, patrol boats, small frigates and destroyers. Broaching-to can be considered as a single wave event. It usually occurs when the wave length is between *1* to *3* ship lengths, and when the wave height is large enough. De Jong et al. (De Jong et al., 2015) showed that the likelihood of broaching increases with the wave steepness. Usually a broaching-to event is preceded by another known and widely analysed phenomenon: surf-riding (Spyrou, 2006; Maki et al., 2010). The vessel is captured by the incoming wave and accelerated to the wave celerity. The vessel then spends a lot of time at one longitudinal position in the wave, typically the front (see the work of Renilson (2014)). At this longitudinal position the destabilizing wave yawing moment grows larger such that the turning moment on the ship from the wave cannot be compensated for by the steering counter-action. The dynamics of this phenomenon is usually very quick and violent: a broach occurs in few seconds, and the vessel's yaw rate can be extremely high. The destabilizing yawing moment is greater at a greater heading angle, but as shown in (De Jong et al., 2015) this does not necessarily increase the likelihood of a broach. The reason for this is that at higher wave incidence angles a surf-ride is less likely, since there is a larger difference in the relative speed between the ship and the wave. Surf-riding and broaching-to are thus strictly connected phenomena. A broach occurs shortly after the onset of a surf-riding: without this precondition in most cases the ship experiences just a periodic motion.

The research presented in this paper aims to investigate the inception of this dangerous dynamic instability phenomena in following seas. Designers and researchers are aware of the circumstances in which a broach could occur, as well as of the kinematics which characterises it. What is still not clear it is the reason why certain ships suffer more than others from broaching-to, and which aspects determine the likelihood of a vessel to lose control in the following sea. This debate is still open and a solution must be sought in order to assess the capabilities of a vessel to manoeuvre at sea, which is a problematic task.

Because of its complexity, the issue of manoeuvring-in-waves of fast vessels is rarely investigated during the design process. As a result of this lack of knowledge, the controllability of small high-speed craft is often entrusted to the masters and the helmsmen who operate the vessel. This is also motivated by the fact that the skills of the mariners are considered more important than the inherent characteristics of the small vessels for their safety. As Conolly explained in (Conolly, 1972) referring to the following sea scenarios, *"mariners tend to be philosophical on this subject, and to accept the problems of following seas as a natural environmental hazard. They rely heavily on individual experiences and would not necessarily all follow the same course of action when confronted by a given set of circumstances"*. However, this was written in 1972, and both technology and the expectations of mariners regarding the design of their vessels have changed since then. Therefore, designers must have sufficient certainties regarding the solutions to adopt in order to prevent, or at least mitigate, the vessel vulnerability to dynamic instabilities. This is of vital importance for a reliable safety assessment of a fast craft sailing in rough sea.

The Dutch rescue boat SAR NH-1816 operated by the Royal Netherlands Sea Rescue Institution (KNRM) was chosen in this work as test case for the investigation of the steering qualities of high-speed craft in the following sea. The NH-1816 is the result of an innovative and versatile design project (Keuning et al., 2011), originating from the upgrade of the rescue vessel Arie Visser converted to the Axe-Bow concept (Keuning, 2006). The Axe-Bow is designed to improve the response of the ship in head waves. The craft is equipped with two water-jets, which facilitate rescue operations and ensure good manoeuvrability, and with two retractable skegs which improve the course stability in the seaway. The main parameters of the vessel and its hull lines are shown respectively in Table 1 and Fig. 1.

One of the most reliable ways to investigate the manoeuvring

characteristics of a vessel is by means of model experiments. However, for manoeuvring-in-wave problems experimental techniques are often complicated and expensive, since the number of model experiments required to cover an adequate range of conditions would be too extensive. Experimental studies on the manoeuvrability of high-speed craft are rare and often restricted to the calm water case (Yasukawa et al., 2016; De Jong et al., 2013; Bonci et al., 2017, 2018). In following sea research, free sailing model tests are generally preferred (Nicholson, 1974; Umeda and Hamamoto, 2000; Renilson and Tuite, 1998; Umeda et al., 2008, 2016), since it is possible to directly assess the vulnerability of a vessel to the onset of broaching-to. Captive model tests in waves are often limited to very few wave and model speed conditions, since they are time consuming and difficult to set-up. However, measuring forces and moments acting on the model in a captive model test generates a deeper understanding into the dynamics of the vessel sailing in the seaway.

Manoeuvring-in-waves numerical simulations are usually carried out in the time domain, since it is possible to describe the high frequency loads in the vertical plane and the low frequency ones in the horizontal plane well. In common state-of-art mathematical tools used for manoeuvring-in-waves applications, the manoeuvrability loads are formulated with calm water models, whereas Froude-Krylov and restoring terms are calculated on the actual wavy submerged geometry. This is a feasible approach for medium-large vessels: the waves are smaller than the vessel size and do not influence the characteristics of the submerged geometry, nor the manoeuvrability loads. This is not applicable for small, fast craft: the waves in which they operate are comparable with the vessel size, therefore the submerged geometry and the hydrodynamic loads change with respect to the position in the waves. Because of this, unified seakeeping and manoeuvrability simulation tools, which directly compute the overall loads acting on the hull at each time step, are recommended in the study of high-speed craft sailing in waves. "*Brute-force*" RANSE solvers are capable of providing an accurate description of the dynamics of the vessel; however, due to the great computational effort required, their utilization in manoeuvring-in-waves problems is not practical. Less accurate potential flow models such as panel methods (BEM) have been demonstrated to be an optimal option between a reliable description of the ship dynamics and a reasonable demand of computational effort.

In this study, captive model tests on the model of the SAR NH-1816 were carried out at the SMB of MARIN in following and stern-quartering waves. The objective was twofold: first, the analysis of the hull and steering loads acting on the vessel when sailing in waves; second, the validation of a 3D BEM in the prediction of such loads. The 3D BEM was then used to investigate the inception of dynamic instabilities in the following sea; the validation of this model allowed both a qualitative and quantitative prediction of the broaching behaviour of the NH-1816.

2. Mathematical model

Unified seakeeping and manoeuvring mathematical models are the state-of-art tools used for manoeuvring-in-waves problems (Bailey et al., 1997; Fossen, 2003; Skejic and Faltinsen, 2008). Both the manoeuvrability and the seakeeping of a vessel must be predicted accurately by

Table 1
Principal parameters of the SAR NH-1816 rescue high speed-craft. The length between was chosen as reference length of the vessel.

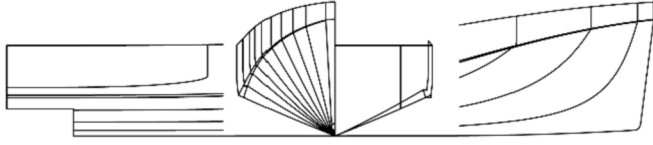| NH-1816 parameters	Symbol	Values
Reference length (length between perpendicular)	L_{PP} or L	*18.37* m
Length overall	L_{OA}	*19.5* m
Overall breadth	B	*5.60* m
Draft at zero speed	T_m	*1.10* m
Longitudinal centre of gravity	LCG	*6.00* m
Mass	m	*34* t
Maximum speed	U_M	35 kts

Fig. 1. Hull buttocks and stations of the SAR NH-1816 craft.

the numerical simulations: the vessel dynamics in the vertical and horizontal planes, as well as its propulsive characteristics, can interact with each other.

In a review of the mathematical methods used to study manoeuvrability in waves, Reed and Beck (2018) considered potential flow methods as an optimal compromise between the accuracy of the results and the range of applicability, when compared to more sophisticated tools (RANSE solvers) or simpler parametric models. In the current study, a 3D BEM was chosen to simulate the motions of a free sailing high-speed craft in stern-quartering seas in the time domain in six degrees of freedom (DOF). The tool was developed mainly by Van Walree (Van Walree, 1999) and De Jong (De Jong, 2011) for both head (De Jong and Van Walree, 2009; De Jong and Van Walree, 2008) and following waves applications (De Jong et al., 2015; De Jong et al., 2013; Van Walree and De Jong, 2011).

Solving a potential flow problem, the 3D BEM evaluates the hydrostatic, Froude-Krylov and hydrodynamic (radiation and diffraction) pressures acting on the ship hull. The viscous effects and the propulsive and steering device loads are calculated using semi-empirical formulations. The hydrodynamic components of the loads are evaluated only on the calm water submerged geometry corresponding to the running equilibrium position of the vessel at the relevant speed. This allows for the linearization of the free surface boundary conditions and the definition of a unique influence function, reducing the computational time albeit with a slightly lower accuracy.

The vessel is initially in its running vertical equilibrium condition while the waves are ramped-up. The propulsion rate is kept constant during the entire simulation. The initial heave and pitch, the wave ramp-up factor, the propulsion rate and the other important simulation parameters are chosen in such a way to give the smoothest start and not to alter the final outcomes of the simulations. The angle of the steering devices is automatically set by the auto-pilot equation given in Equation (1).

$$\delta = b_{\delta\psi}\, r + c_{\delta\psi}\, \psi \tag{1}$$

The auto-pilot is meant to keep the initial course direction of the vessel correcting the deviation in heading ψ and its rate of change r. The main characteristics of the vessel steering are shown in Table 2.

All the motions and loads refer to the ship-fixed coordinate system in Fig. 2, with origin at the ship centre of gravity G. The motion equations in surge, sway, roll and yaw are given in Equations (2)–(5) in dimensional form.

$$(m + m_x)\dot{u} + mvr = X_H + X_W + X_R \tag{2}$$

$$(m + m_y)\dot{v} \text{ - } mur + m_y\alpha_x\dot{r} = Y_H + Y_W + Y_R \tag{3}$$

$$(I_x + J_x)\dot{p} = K_H + K_W + K_R \tag{4}$$

Table 2
Summary of the main steering parameters of the waterjets of the SAR NH-1816 craft. These characteristics are taken by the previous work of De Jong et al. (Keuning et al., 2011) on the same vessel.

Steering parameters	Symbol	Value
Autopilot proportional coefficient	$c_{\delta\psi}$	3 deg/deg
Autopilot damping coefficient	$b_{\delta\psi}$	9.49 deg/(deg/s)
Steering rotation velocity	δ	10 deg/s
Maximum steering angle	δ_M	23 deg

$$(I_z + J_z)\dot{r} + m_y\alpha_x\dot{v} = N_H + N_W + N_R \tag{5}$$

The equations in heave and pitch are not considered. However, the vertical and components of the loads and thus the actual trim and sink/rise of the craft in the waves are maintained by the 3D BEM in a quasi-static manner, because the variations in submerged geometry due to the motions in heave and pitch influence the manoeuvring of the vessel.

The loads acting on the vessel are divided into: hull loads (both hydrodynamic and hydrostatic subscript H); wave loads (subscript W); and the propulsive and steering forces provided by the waterjets (subscript R). Each of these terms depends on the vessel speed, the wave characteristics, the longitudinal location of the ship in the waves and its running attitude which defines its submerged geometry in the waves. The hull component of the loads acting on the ship can be described using the derivatives of the loads with respect to the motions (hydrodynamic coefficients), as in Equations (6)–(9).

$$X'_H = R'_T(u) + X'_{vv}v'^2 \tag{6}$$

$$Y'_H = Y'_v v' + (Y'_r - m')r' + Y'_\Phi\Phi' \tag{7}$$

$$K'_H = (K^{*'}_\Phi - m'GM'_T)\Phi' + K'_v v' + K'_r r' \tag{8}$$

$$N'_H = N'_v v' + N'_r r' + N'_\Phi\Phi' \tag{9}$$

These equations are given in non-dimensional form; all the non-dimensional quantities are obtained dividing them with the correct combination of water density ρ, ship reference length L and forward speed U according to the convention used for manoeuvring (see (Principles of Naval Archi, 1988)), and hereby denoted with the superscript '.

In a similar way, it is possible to linearize the wave sway force, roll and yaw moments with respect to the wave incidence angle μ, as done in Equations (10) to 12.

$$Y'_W = Y'_\mu\, \mu \tag{10}$$

$$K'_W = K'_\mu\, \mu \tag{11}$$

$$N'_W = N'_\mu\, \mu \tag{12}$$

The NH-1816 rescue vessel taken as object of the investigation is equipped with waterjets. The forces and moments generated by the waterjets are calculated in the simulations according to the Equations (13)–(16).

$$X_R = \rho Q(u_{NOZ} - c_M u cos\beta_R)cos\delta \tag{13}$$

$$Y_R = \rho Q(u_{NOZ} - c_M u cos\beta_R)sin\delta = Y_\delta\delta \tag{14}$$

$$K_R = YR \cdot z_{NOZ} = K_\delta\delta \tag{15}$$

$$N_R = -YR \cdot x_{NOZ} = N_\delta\delta \tag{16}$$

In this paper, the steering sway force, roll and yaw moment will be notated by the terms $Y_\delta\delta$, $K_\delta\delta$ and $N_\delta\delta$, i.e. making use of the manoeuvring notation for the steering force and moment derivatives with respect to the steering angle δ.

The term Q denotes the flow rate through the waterjet duct, which depends on the impeller rate; β_R is the flow incidence angle at the waterjet inlet; u_{NOZ} is the flow speed at the waterjet nozzle, located at the longitudinal and vertical coordinate x_{NOZ} and z_{NOZ}; c_M is an empirical coefficient representing the flow momentum due to the impeller suction.

3. The prediction of the hull loads in following and stern-quartering waves

In this Section, the capability of the 3D BEM for prediction of the manoeuvring loads is assessed. The calculated loads are compared with the results from captive model tests carried out at the SMB of MARIN both in calm water and in regular following and stern-quartering waves.
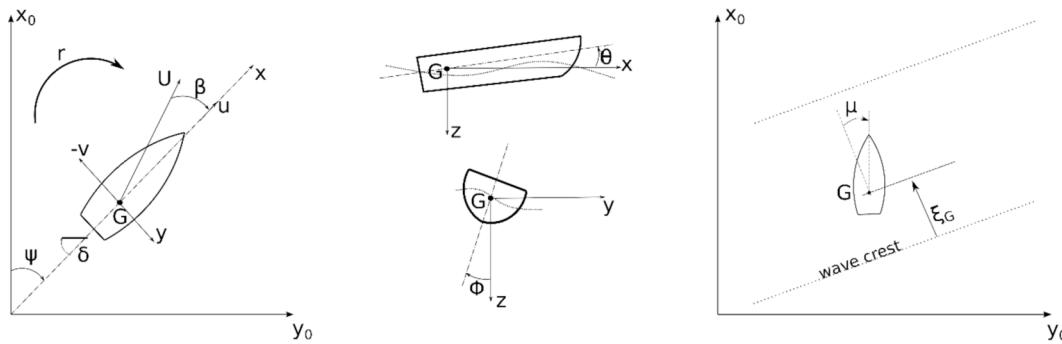
Fig. 2. Earth-fixed $E^e = (x_0, y_0, z_0)$ and ship-fixed $E^b = (x, y, z)$ reference coordinate systems. The origin of the ship-fixed coordinate system is located in the centre of gravity G of the vessel. The ship-fixed is a yawed-only frame: axis y, pointing starboard, and axis x, pointing ship forward, lay on the horizontal plane; axis z points constantly downwards. The hydrostatic and gravity forces do not contribute to the manoeuvring loads acting on the horizontal plane. On the right, the definition of the location of the vessel in the wave is shown in terms of the quantity ξ_G, which represents the distance in the wave propagation direction of the centre of gravity G from the nearest incoming wave crest. $\xi_G/\lambda = 0$ or 1 means that the origin of the vessel is located on the wave crest; $0 < \xi_G/\lambda < 0.5$ on the wave front; $\xi_G/\lambda = 0.5$ on the wave trough, $0.5 < \xi_G/\lambda < 1$ on the wave back.

A photograph of the ship model used in the tests is shown in Fig. 3.

The BEM used for the simulation of the ship motions is a blended method: the inflow potential on each of the hull panels is composed of the radiation potential and the Froude-Krylov + diffraction potential. It is impossible in a free-sailing vessel simulation to clearly separate the effects of the loads in waves, as written in Equations (2)–(5). In order to investigate the numerical prediction of the manoeuvring forces and moments, the same experimental captive model tests were reproduced numerically; therefore, the single contributions to the total loads can be computed and compared with the experimental data.

The experiments in regular waves were carried out at constant steepness $H/\lambda = 0.06$, taken as the upper limit to ensure good quality waves and to avoid wave breaking. A number of wave lengths and model speeds were chosen in order to realize conditions of following waves at low encounter frequency where the waves slowly overtake the model. The experimental set-up allowed the model to move in heave and pitch, thus assuming its natural vertical position in the wave. This is an important requirement of the experimental set-up, since the loads in the waves also depend on the vertical position of the model in waves. The loads measured in this model test campaign refer to the bare hull without skegs. The uncertainty of the measured data is expressed by the random errors (precision limits) evaluated from *12* repetitions of a single run for each case.

The particulars of the tests are summarised in Table 3. Fig. 4 shows two pictures of a measurement run carried out at the SMB. Three different types of experiments were carried out:

Table 3
Summary of captive model tests conditions at the SMB.

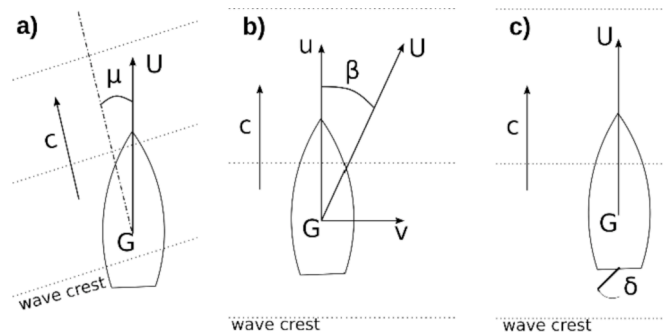| Condition	Fr	λ/L	H/λ
1	0.38	1	0.06
2	0.38	1.5	
3	0.48	1.5	
4	0.48	2	
5	0.53	2	

Fig. 4. Schematic representation of the captive model tests performed at the SMB of MARIN as described in the text.

a) *Tests at wave incidence angle with zero sway velocity.* The wave induced loads were measured at different wave incidence angles up to *25* degrees. At this stage the model had zero sway velocity, see Fig. 4, and hence there was no contribution to the sway force or yaw moment from the sway velocity. Thus, the only loads which were measured were due to the wave.

b) *Tests at pure sway motion in following waves.* The sway velocity induced loads were measured while the model was running with constant drift in waves. The incidence angle between the direction of the waves and the ship longitudinal axis was zero, see Fig. 4, and hence there was no contribution from the wave to the sway force or yaw moment. Thus, the only loads which were measured were due to the sway velocity.

c) *Tests with waterjets steering angles.* The steering loads of the waterjets were measured in waves at different steering angles. In this condition the sway motion and the wave incidence angle were zero, and hence there was no contribution to the loads from either the sway motion or the wave, see Fig. 4. Thus, the only loads which were measured were due to the waterjet steering angle.
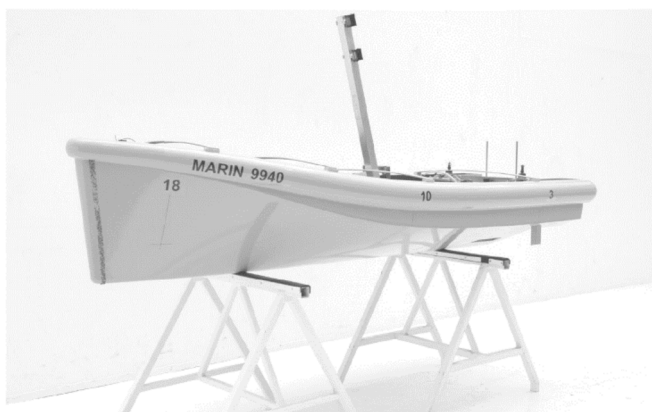

Fig. 3. Model of the SAR NH-1816 used during the experimental campaign at SMB of MARIN.

Fig. 5 shows a picture taken during a run in following waves. The loads due to the sway velocity and the waterjet steering angle were also evaluated in calm water at the same model speeds as used for the tests in waves in order to make a comparison between the condition in calm water and the one in waves.

The results obtained from the tests are presented in terms of hydrodynamic coefficients or loads as functions of the position of the longitudinal centre of gravity, *G*, of the vessel in the waves, denoted using the non-dimensional parameter ξ_G/λ defined in Fig. 2. The results are presented in non-dimensional form, as shown in Equations (17)–20 for the force *F*, moment *M*, sway speed *v* and yaw velocity *r*:

$$F' = F/(0.5\rho U^2 L^2) \tag{17}$$

$$M' = M/(0.5\rho U^2 L^3) \tag{18}$$

$$v' = v/U \tag{19}$$

$$r' = r\,L/U \tag{20}$$

The coefficients were obtained at each location ξ_G/λ by the least squares linear fitting of the measured non-dimensional values, as function of the non-dimensional velocity components or the angles expressed in radians. Fig. 6 shows an example of the fitting of the yaw moment due to sway in calm water and in two locations in waves for one condition tested.

The quality of the fitting is estimated by calculating the uncertainty of each measurement run (ITTC Recommended Procedure no. 7.5-02-06.04 (ITTC, 2014)) and the Standard Estimation Error (SEE) of the fitting line (Coleman and Steele, 1999). The total coefficient uncertainty is visualized by means of error bars on each coefficients value. The same methodology can be found in (Bonci et al., 2019).
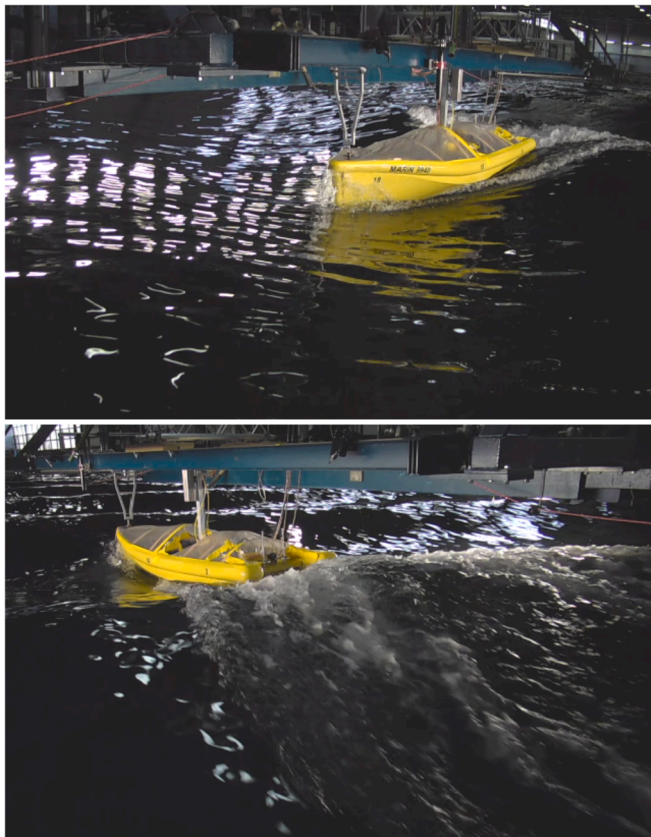

Fig. 5. Bow and stern views taken at the same instant of a captive test run at the SMB of MARIN, in stern-portside-quartering waves. $\lambda/L = 2$; Fr = 0.48; $\mu = 25$ deg.
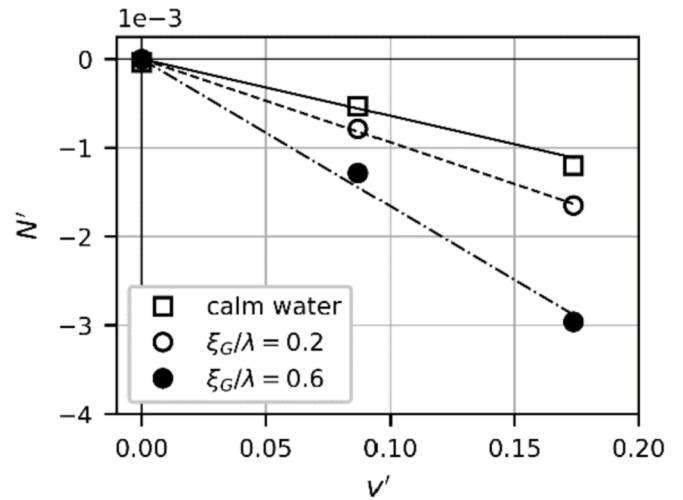

Fig. 6. Measurement data and fitting in calm water and in waves (two locations ξ_G/λ are plotted) of the non-dimensional yaw moment due to sway as function of the non-dimensional sway velocity. The data refer to the runs at Fr = 0.48.

3.1. Empirical description of the manoeuvring forces and moments

The experimental results can be used to formulate an empirical description of the forces and moments due to manoeuvring at different combinations of vessel Froude number and wave lengths. It is important that the 3D BEM can also predict the forces and moments acting on the hull in several other conditions different than the cases considered in the model tests. The same approach can be found in (Bonci et al., 2019).

For this purpose, it is useful to express concisely the coefficients in waves using very few parameters, i.e. the amplitude, the mean value and the phase of the sinusoidal signal of the relevant quantities, as shown in Fig. 7. This approximation is valid under the hypothesis of linearity between the exciting wave and the output load which fits the forces and moments due to manoeuvring well.

This method assumes linearity between the wave and the loads acting on the hull; this hypothesis approximates reasonably the measured data. Fig. 8 compares the measured data for one condition in waves tested and the respective sinusoidal fitting.

Those terms can be obtained by least square fitting of the sinusoidal signals as functions of the location of the ship in the wave, ξ_G/λ. Each coefficient can be then expressed as in Equation (21), with the term Y'_v
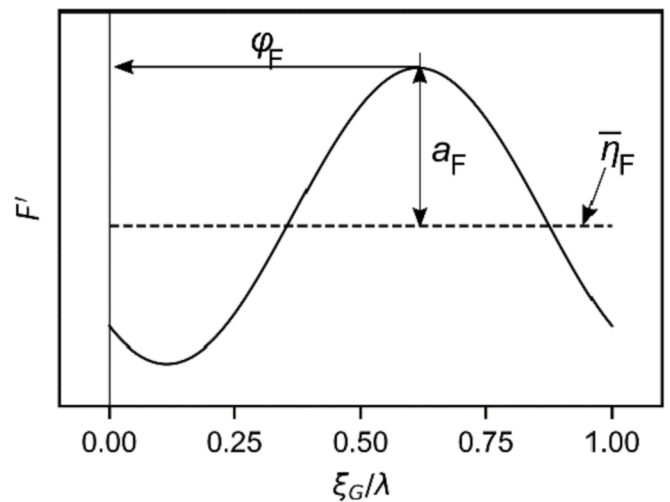

Fig. 7. Generic non-dimensional quantity F′ acting on the vessel seen as a sinusoidal function. The amplitude a_F, the mean value η_F and the phase φ_F are defined as shown.
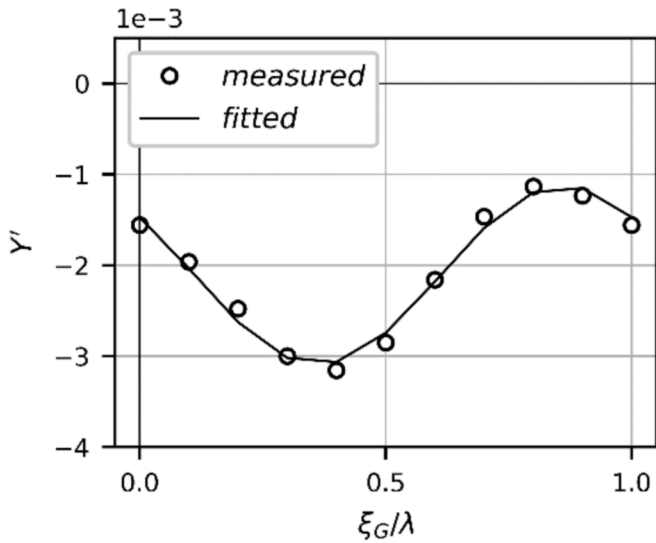
Fig. 8. Sinusoidal fitting of the non-dimensional sway velocity induced sway force measured at SMB for one run in regular waves. $\lambda/L = 1.5$; $Fr = 0.38$; $\beta = 5$ deg; $H/\lambda = 0.06$.

taken as example.

$$Y_v = a'_{Yv} \cos(2\pi\ \xi_G/\lambda + \varphi'_{Yv}) + \eta'_{Yv} \tag{21}$$

The amplitude, phase and mean value can be plotted as functions of Froude number and wave length, for every condition tested. The values of amplitude, phase and mean of the experimental cases can be fitted using a plane, as shown in Fig. 9; thanks to this plane, the coefficients can be expressed using the plane polynomial terms, as in Equation (22) for the mean value of the coefficient Y'_v.

$$\eta'_{Yv} = p_0 + p_1\ Fr + p_2\ \lambda/L \tag{22}$$

The terms p_0, p_1 and p_2 are the coefficients of the plane equation. A planar fit was chosen as a first approximation of the coefficients in waves.

The empirical description was used to correct the numerical prediction of the loads predicted using the 3D BEM. The captive model tests were reproduced numerically with the 3D BEM for the same conditions tested in the experiments. As with the model test results, the coefficients obtained numerically using the 3D BEM can be used to define a numerical description by fitting the data with a plane, as shown in Fig. 9 for
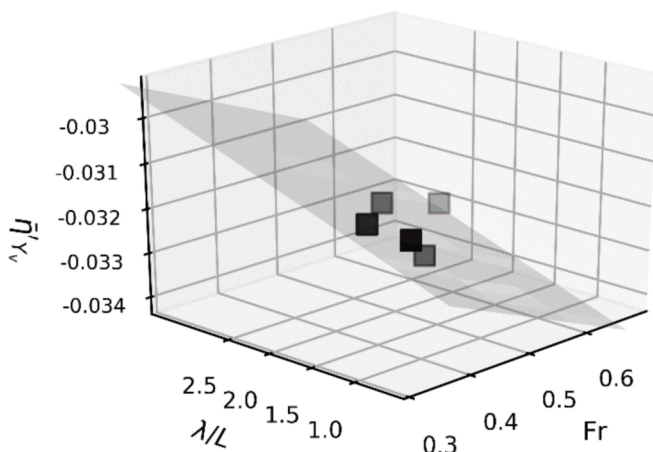

Fig. 9. Planar fit of the mean value of the manoeuvring coefficient Y'_v. The black squares are the measured values; the grey plane fits these data within the computational domain of Fr and λ/L.

the experimental cases. The differences between the experimental and numerical plane fits can be calculated for every Fr - λ/L combination, and therefore used to correct the 3D BEM prediction.

This correction allows an imperfect but reasonable agreement with the experimental results for a wide range of forward speeds and wave lengths. The correction depends on how well the terms are distributed over the plane, and on how different the initial numerical coefficients are from the experimental measurements. The complete numerical-experimental comparisons of amplitude a, phase φ and mean value η are shown in the Appendix, for the coefficients induced by the waves and the sway velocity of the vessel.

3.2. Test a): loads due to the wave

The wave loads were computed using the 3D BEM considering the Froude-Krylov pressures on the actual wavy submerged geometry. Since the wave exciting forces are mainly potential, the boundary element mathematical methods are expected to predict these loads rather well. Fig. 10 shows the uncorrected numerical and the measured wave loads, confirming the initial expectations. Some discrepancies can still be observed, especially in the roll moment; however, the 3D BEM provides a reasonable prediction of the wave excitation. Therefore, the predictions from the 3D BEM do not need to be corrected in this case. A comparison between the measured and predicted wave loads for a single run is shown in Fig. 10. A more detailed comparison of the measured and predicted wave surge force X'_W and wave coefficients Y'_μ, K'_μ and N'_μ is given in the Appendix.

3.3. Test b): loads due to sway velocity

It is much more difficult to accurately predict the manoeuvring forces and moments, such as the forces caused by the sway velocity, using potential methods. The forces and moments acting on a hard-chine craft due to sway velocity are governed by complex phenomena such as spray generation, and flow separation at the chine and at the transom. Moreover, the presence of the wave increases the complexity of the phenomena acting on the hull. The results of the predictions obtained using the 3D BEM were then corrected as explained in Section 3.1. The comparison between the corrected BEM and measured sway hydrodynamic coefficients is shown in Fig. 11 for one case. A wider and more detailed comparison is given in Appendix.

When a free running ship is sailing in following waves it is subjected to large fluctuations in its surge velocity. In extreme cases the ship is forced to travel at wave speed, known as surf-riding. As discussed above, surf-riding is a prerequisite of broaching-to. A good match between the measured and predicted loads from the captive model tests is not enough to judge the behaviour of the vessel when it is freely running in a seaway, because in the model tests the vessel forward speed is kept constant whereas it is variable in the free running case. The 3D BEM accounts for the variation of the loads due to the change in forward speed, which gives the correction applied at the initial speed. Therefore, it is of paramount importance that the 3D BEM is capable of predicting the change in the hydrodynamic loads due to forward speed. Fig. 12 depicts the comparison between the measured and predicted coefficients Y'_v, K'_v and N'_v in calm water as a function of Froude number over the speed range investigated. The comparison shows that the 3D BEM can be used to qualitatively predict the trend of the hydrodynamic coefficients with respect to the forward velocity.

3.4. Test c): waterjet steering loads

The steering loads generated by the waterjets at different deflection angles, δ, were measured during the model tests, both in calm water and in waves. Fig. 13 shows the waterjet arrangements during the experimental campaign. The RPM of the waterjet impellers were set to match the resistance in calm water at speed.
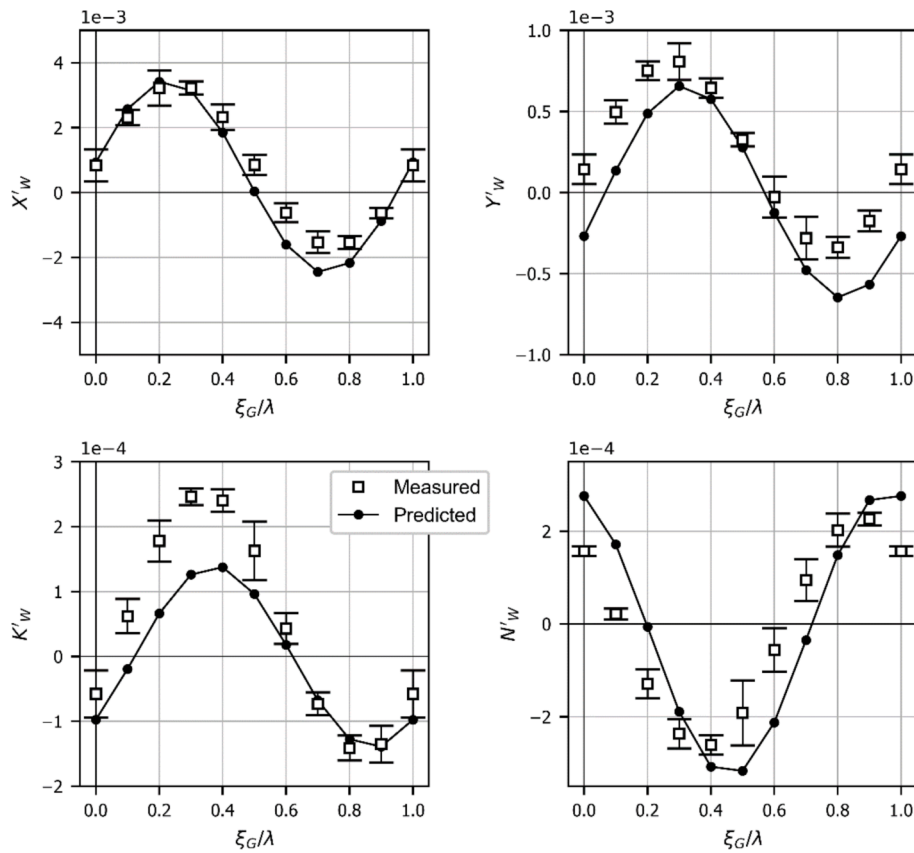
Fig. 10. Comparison between wave surge, sway forces and roll, yaw moments measured and predicted. $\lambda/L = 1$; $Fr = 0.38$; $\mu = 10$ deg.
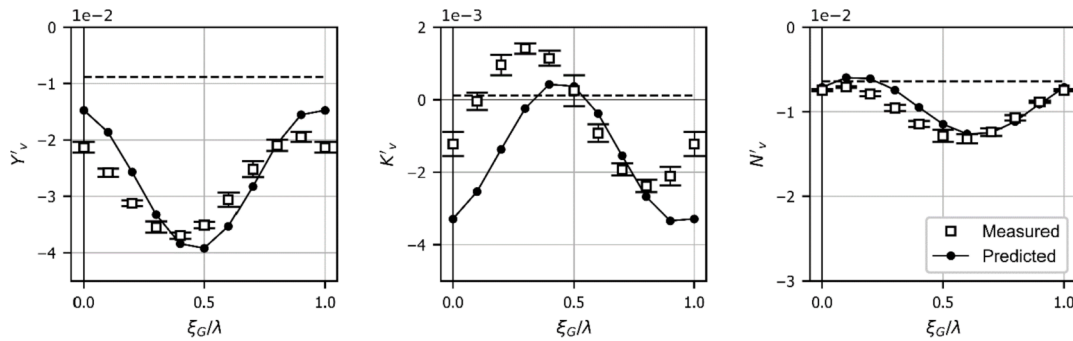

Fig. 11. Sway velocity induced coefficients in sway, roll and yaw. Comparison between the measured coefficients and those predicted numerically. $\lambda/L = 1.5$; $Fr = 0.38$.
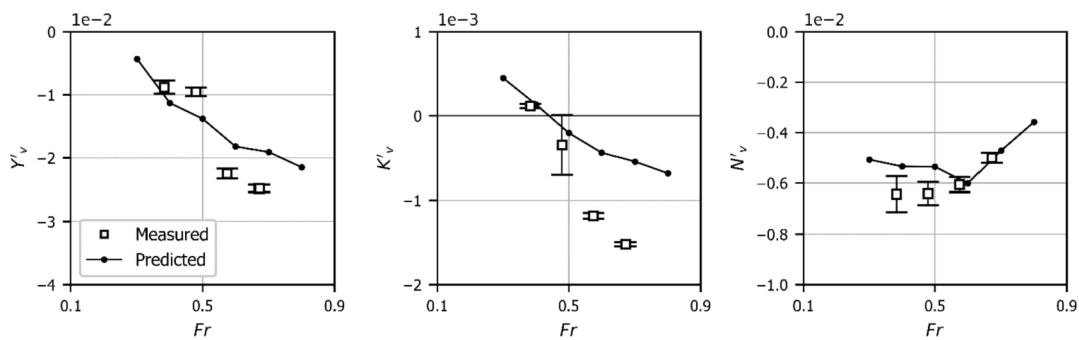

Fig. 12. Comparison of the measured and predicted values of the coefficients Y'_v, K'_v and N'_v obtained in calm water as a function of Froude number.

Fig. 13. View of the waterjets arrangement on the NH-1816 model.

The results in waves are shown in Fig. 14 in terms of the derivatives of side force Y'_δ, roll and yaw moments K'_δ and N'_δ for one experimental case. The steering coefficients in the following waves are very similar to the calm water values, except for the roll moment.; however, the difference is rather small when compared to the other loads. This suggests that the waterjets performance in a seaway are very similar to its performances in calm water. This is different to what could happen to a propeller + rudder configuration, where the orbital velocities can reduce the effectiveness of the rudder, and in extreme cases rudder emersion can occur. Waterjets are less subjected to wave induced inflow velocities components or submergence.

The coefficients measured in the experiments were compared in Fig. 15 with the mathematical model of the waterjet loads used during the simulations at different forward speeds, as done for the coefficients in sway.

The waterjets mathematical model summarised by Equations (13)–(16) is adequate in capturing the steering forces. The waterjets are however subjected to the variation of surge speed of the vessel when surf-riding, since the flow speed at the waterjets inlet change, while the RPM is kept constant. This effect is not highlighted in the captive tests, since the forward speed is constant; however, the surge effect is taken into account by the waterjet model.

3.5. Loads due to yaw velocity

Different consideration must be made for the yaw velocity induced coefficients Y'_r, K'_r and N'_r. It is very hard to obtain these coefficients in regular following waves. In the past Renilson (Renilson, 1981; Renilson and Driscoll, 1982), Matsuda and Umeda (2000) proposed experimental

methodologies to obtain these coefficients in waves. The problem is that when a vessel is turning with a yaw velocity $r(t)$, its heading $\psi(t)$ is also changing, thus modifying the actual wave incidence angle $\mu(t)$. It is therefore hard to separate the wave and yaw velocity effects. This is in principle possible as explained by Equation (23), which refers to the total yaw moment when the vessel turns in waves in the absence of sway velocity.

$$N = N_\mu\mu(t) + N_r r(t) = N_\mu(\mu - \psi(t)) + N_r r(t) = N_\mu(\mu - \int r(t)dt) + N_r r(t) \quad (23)$$

However, the most difficult task is to correctly set the longitudinal location of the model in the wave. This can be done by moving the carriage at the same speed as the wave crest celerity, thus performing pure yaw oscillation tests at the same longitudinal wave location. This would require a significant number of model runs, and it was not feasible for the present model test campaign.

As an approximation, the values of the yaw velocity coefficients used were those obtained in calm water. The prediction of these terms using the current 3D BEM technique was validated in the work of De Jong et al. (De Jong et al., 2013). Fig. 16 shows the values of the coefficients Y'_r, K'_r and N'_r as functions of Froude number in calm water over the speed range investigated.

3.6. Wave steepness effect

The experimental campaign was carried out at a single wave steepness $H/\lambda = 0.06$. It is known that the occurrences of dynamic instabilities in the following sea are more frequent at steeper waves. Therefore, it is necessary to perform simulations at a steepness higher than *0.06*. The 3D BEM takes into account the effect of steepness for the computation of the wave and hydrodynamic loads.

Every load in the wave can be seen as a sinusoidal curve function of the term ξ_G/λ. Then, every sinusoidal curve has its own amplitude, mean value and phase with respect to the exciting wave: a modification of wave steepness has the effect of changing these parameters. This is taken into account also into the correction of the predicted loads due to sway velocity.

The effect of the wave steepness on the manoeuvring loads can be significant, since the change in the submerged geometry is large, hence greatly affecting the distribution of the pressure over the hull. Fig. 17 shows the predicted effect of the steepness on the amplitude and mean value of the hydrodynamic coefficient N'_v. A change of wave steepness affects only the amplitude and the mean value of the loads, not the phase.

4. The inception of broaching-to

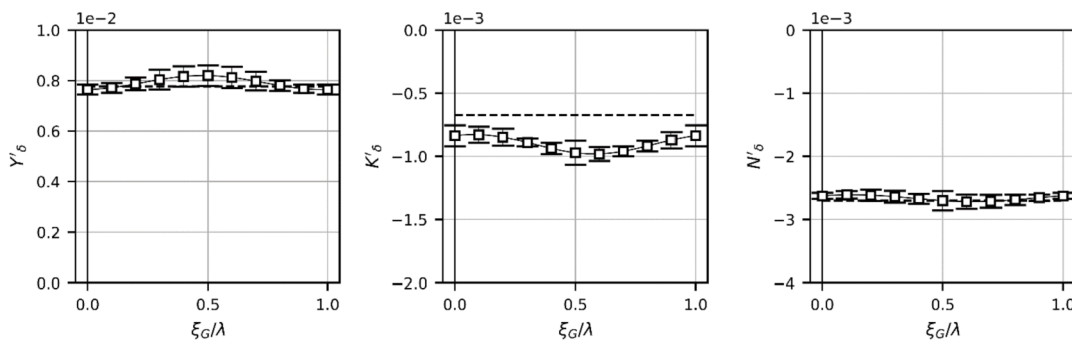The most important steering qualities of the high-speed craft can be summarised by two characteristics:

Fig. 14. Comparison between the measured values of the waterjet coefficients Y_δ, K_δ and N_δ in following waves ($\lambda/L = 1$, Fr = 0.38); the horizontal dashed line refers to the value of the coefficients in calm water at Fr = 0.38.

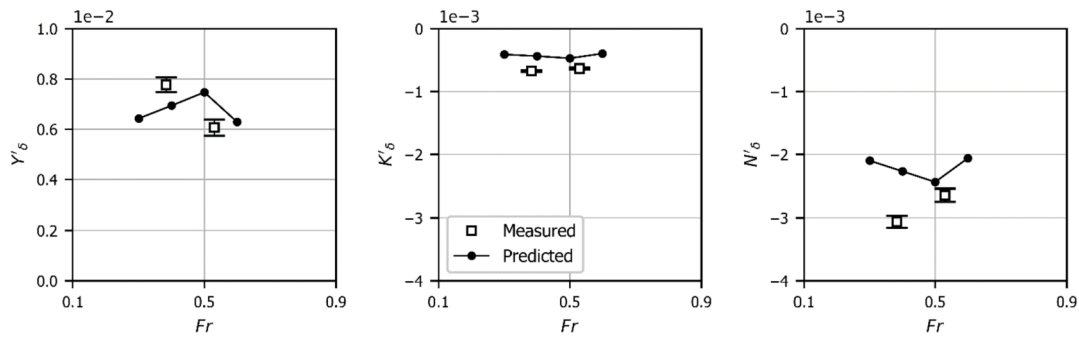**Fig. 15.** Comparison between the measured and predicted values of the waterjet coefficients Y_δ, K_δ and N_δ in calm water as a function of Froude number.
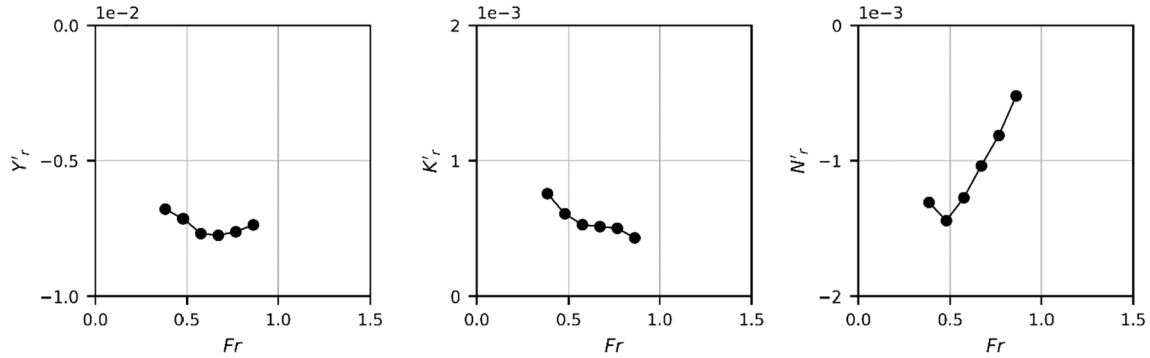

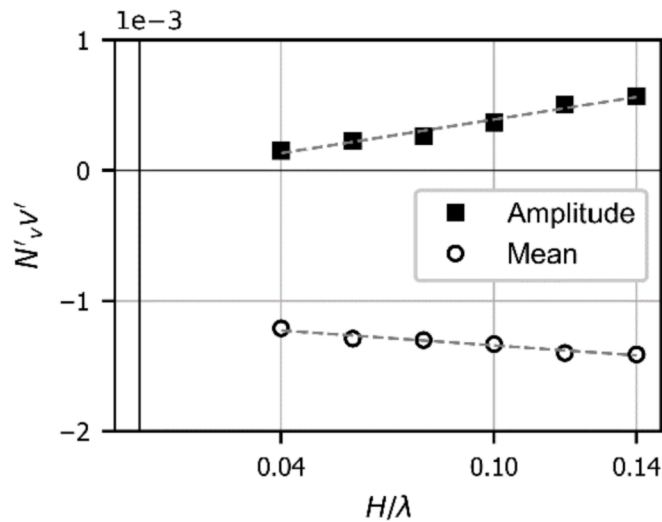**Fig. 16.** Numerical values of the hydrodynamic coefficients Y_r, K_r and N_r in calm water.

Fig. 17. Amplitude and mean value of the sway induced yaw moment as function of the wave steepness. The values are obtained by means of numerical simulations, for the condition of $\lambda/L = 2$, $Fr = 0.48$, $\beta = 5$ deg.

1. The ability to maintain the desired course with the minimum steering effort after a disturbance (course keeping ability);
2. The ability to change heading quickly and in a limited amount of longitudinal displacement (turning ability).

In this work, these two different, but related, aspects of the manoeuvrability of high-speed craft have been investigated in relation to their effect on the inceptions of broaching phenomena in stern-quartering waves. The elements investigated independently are:

5. Directional stability and effectiveness of the steering devices

Both these elements will affect the steering qualities identified above, and hence these were varied independently to study their effect on the inception of broaching in stern-quarter seas. The effectiveness of the steering can be modified by increasing the total steering force provided by the control devices. The directional stability of the high-speed craft was modified by considering the well-known index C' (Principles of Naval Archi, 1988) in Equation (24):

$$C' = N'_r Y'_v - (Y'_r - m') N'_v \tag{24}$$

The investigation was made up of four different designs which originate from the bare hull of the NH-1816 as summarised in Table 4. Each of the designs had different directional stability and steering ability and these are denoted as follows:

A. The bare hull of the NH-1816 is considered without modification;
B. The directional stability of the NH-1816 was improved by artificially modifying the linear hydrodynamic coefficients due to sway velocity Y'_v, N'_v and due to yaw velocity Y'_r, N'_r;

Table 4
Summary of wave incidence, drift and steering angles tested for each condition of the experimental campaign in waves and in calm water.

Test	Description	Values [deg]
a)	Tests at wave incidence angle without sway velocity	$\mu = 0, 5, 10$ for conditions 2 and 4 $\mu = 0, 5, 10, 15, 20, 25$ for conditions 1, 3 and 5
b)	Tests at pure sway motion in following waves	$\beta = 0, 5, 10$ for all conditions
c)	Tests with waterjets steering angles	$\delta = 0, 5, 10, 20$ only conditions 1 and 5 tested
–	Pure drift tests in calm water	$\beta = 0, 5, 10$ for $Fr = 0.38, 0.48, 0.53$
–	Tests with waterjets steering angle in calm water	$\delta = 0, 5, 10, 20$ for $Fr = 0.38, 0.53$

Table 5
Scheme of the four designs with the variation in the relevant coefficients.

Design A		Design B	
No coefficients variation		Y_v, N_r	Increased by 25%
		Y_r, N_v	Decreased by 25%
Design C		*Design D*	
Y_δ, N_δ	Increased by 25%	Y_v, N_r	Increased by 25%
		Y_r, N_v	Decreased by 25%
		Y_δ, N_δ	Increased by 25%

C. The steering ability of the vessel was improved by artificially increasing the steering side force, resulting in greater coefficients Y'_δ, K'_δ and N'_δ;

D. Both the directional stability and steering ability were improved at the same time.

For designs B and D, the coefficients Y'_r and N'_v were decreased by 25%, and the coefficients N'_r and Y'_v were increased by 25%. Also the roll coefficients K'_v and K'_r were increased by 25%, in order to realistically simulate the presence of the skegs, i.e. a condition of bare hull + appendages. The appendages were not added directly in the simulations in order to avoid the induced effects due to the fluctuations of the forward speed and the presence of the wave. In designs C and D, the steering coefficients Y'_δ, K'_δ and N'_δ were increased by 25%. These percentages have been chosen to simulate a feasible net increase of steering force available for the ship.

Although present in the numerical simulations, the heel induced coefficients Y'_Φ and N'_Φ were not considered in this investigation. The effect of those terms on the broaching-to inception and on the manoeuvring characteristics of fast vessels in calm water has already been discussed in previous work (Bonci et al., 2018, 2019; Oltmann, 1993; Hashimoto et al., 2011; Yasukawa and Yoshimura, 2014; Renilson and Tuite, 1995, 1996, 1997). For the purpose of this study, only the more classic sway-yaw dynamics was taken into consideration to relate the dynamic stability of the high-speed craft to its steering qualities.

It must be noted that the modification of the coefficients was realistic but not physical. The hull coefficients were changed without considering a relative change in hull form, or an addition of appendages. The steering force was increased without considering the effect that this would have on the surge dynamics of the vessel, or that an increase in the waterjet steering forces would be achieved only by accelerating and increasing the waterjet impeller rate. The surge dynamic of the vessel was not modified so that it was possible to make a net comparison between different steering qualities of the vessel, disregarding the induced modifications on the vessel that would have an influence on the ship behaviour at sea. A summary of the main aspects of the four designs is given in Table 5.

Simulations in regular waves for the four designs were carried out at constant wave steepness, $H/\lambda = 0.08$, for a range of Froude numbers from *0.32* and *0.59*, and wave lengths from *1* to *3.5* ship lengths. The vessel auto-pilot was set to maintain the initial heading of *20* degrees to the wave direction. In total, these amount to 7*8*4 simulations, which were ran in the time domain over a time duration which equals the sum the wave ramp-up period (set to about 60 s) and two wave encounter periods. The resulting time traces have been analysed to classify the behaviour of the model in each of 4 categories: periodic motion, surf-riding, broaching-to and capsize. The criteria for putting it in one of these categories are defined in Table 6; four examples of the occurrence of these dynamic instability events are shown in Fig. 18. Periodic-motion is implicitly defined as the non-occurrence of the other three phenomena.

The results of this analysis are presented in Fig. 19 for the four vessel designs. The results are presented in terms of the λ/L ratio and the Froude number. The conditions where a dynamic instability

Table 6
Criteria for the detection of the main instability events treated in this work, surf-riding, broaching-to and capsize.

Instability event	Detection
Surf-riding	$U \geq c$
Broaching-to	$\delta = \delta_{MAX}$, $r > 0$, $\dot{r} > 0$
Capsize	$\Phi > 90$ deg

phenomenon occurs highlight a "broaching zone". This approach was firstly developed by Nicholson (1974), and further used in many of the later works on this topic (Renilson, 1981; Renilson and Driscoll, 1982; De Jong et al., 2013, 2015; Umeda and Hamamoto, 2000; Renilson and Tuite, 1998; Umeda et al., 2008, 2016; Hashimoto et al., 2004).

Design A is the base condition of the bare hull vessel, showing a rather extended broaching zone covering almost the entire range of wave lengths and speeds simulated. Both the design with the increase in directional stability (B) and the design with the increased steering ability (C) show a reduced broaching zone. Design C has a smaller broaching zone than Design B, suggesting that, in this case, increasing the steering ability has a greater effect on reducing the broaching tendency than increasing the directional stability. However, a greater steering force would induce a roll moment in the same direction of the ship roll during the broaching-to inception, increasing the risk of capsize. This is not counter-acted by the auto-pilot, which keeps into account only the vessel heading. The combination the two (Design D)
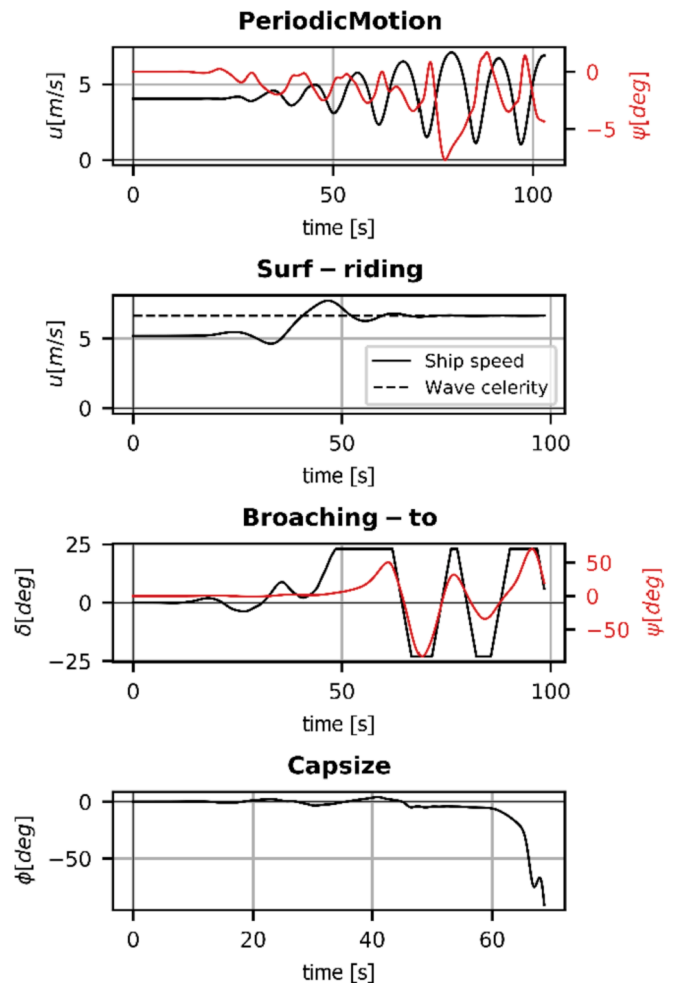

Fig. 18. Four examples of possible phenomena happening in following seas: periodic motion (non-occurrence of a dynamic instability event), surf-riding, broaching-to and capsize.
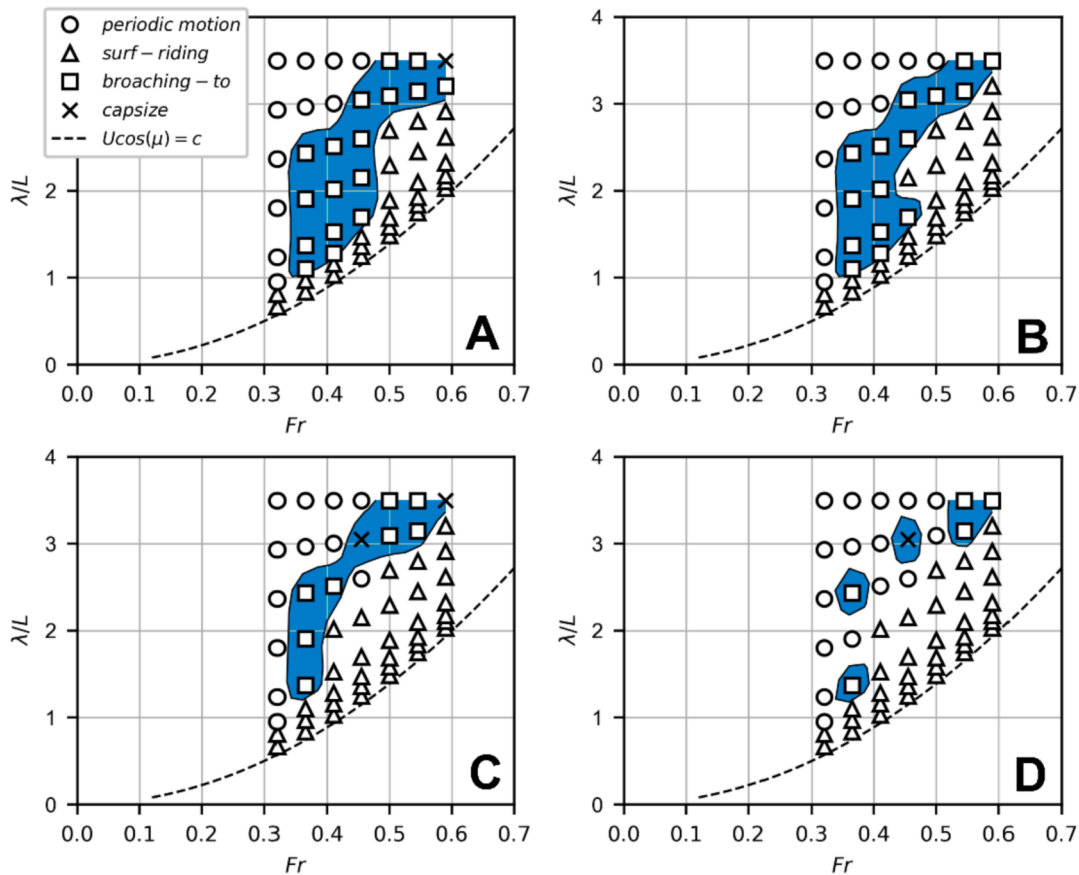
Fig. 19. Broaching zone plots for the four designs A-D. The occurrence of broaching is highlighted within the coloured region; periodic motions, surf-riding and capsize are also noted by different symbols. Simulations were carried out above the Ucos(μ) = c line, i.e. where the waves are travelling faster than the initial speed of the vessel, and hence overtaking the vessel.

results in a greater improvement. This suggests that a design both more steer effective and more directional stable would reduce the tendency of the vessel to broach in a following and stern-quartering sea.

6. Discussion

From the results in Fig. 19, it can be seen that an increase in the directional stability and in the steering ability are both beneficial to reduce the broaching tendency of the high-speed craft in following and stern-quartering waves. Increasing the vessel directional stability decreases the tendency to broach, but a more steer effective design decreases even further this tendency.

Fig. 20 shows the comparison of the simulation time histories in the same condition for the three Designs A, B and C. The initial speed of the vessel corresponds to $Fr = 0.41$ and the wavelength to ship length ratio is *1.53*. Although the broach takes more time to build-up for the case with the increased directional stability (B), than for the original design (A), the increase in directional stability does not prevent a broach from occurring. On the other hand, the increase in steering effectiveness (C) does prevent the broach from occurring.

For higher initial forward speeds and the longer waves, the design with the increased steering ability (Design C) does not show the same benefits which are present at lower speeds and lower wavelengths. This is because the waves are longer and higher and so are more powerful, and an increase in steering force alone is not capable to fully counter-acting the wave induced yawing moment.

Fig. 21 shows a comparison of the simulation time histories for the three Designs A, B and C, but this time at a higher initial forward speed corresponding to $Fr = 0.5$, and a longer wavelength corresponding to a wavelength to ship length ratio of *3.5*. For this higher initial forward

speed, it is possible to observe that the for original design and the one with enhanced steering a broach occurs, whereas this does not happen for the more directional stable design.

Fig. 22 shows a comparison of the simulation time histories for Design B and Design C, with both increased directional stability and steering effectiveness. The initial forward speed corresponds to $Fr = 0.41$ and the wavelength to ship length ratio is *2.51*. As with the conditions shown in Fig. 19, broaching occurs less for Design D: broaching occurs at both Design B and C but not for Design D.

For the results presented above, the capabilities of the vessel have been modified assuming a realistic change in directional stability which would be expected due to the addition of skegs. To investigate this issue in more detail, the effect of directional stability was investigated by modifying the linear coefficients more to increase the vessel's directional stability further.

Fig. 23 shows the three different *C-indexes* in calm water as function of Froude number. These indexes were obtained by modifying the sway and yaw velocity induced coefficients by *25%* as done previously, and further by *50%*. The original design corresponding to Design A, C_0, has negative *C-index*, meaning that the vessel is course unstable in calm water. Unlike the case for a big displacement ship, this is not a result of a bad design: a negative *C-index* on a high-speed craft is not rare because these vessels need to have good manoeuvring and turning ability.

Fig. 24 shows a comparison of the broaching-to plots for the designs obtained with the progressive changes in the manoeuvring coefficients, resulting in the three different directional stability indexes C'_0 *(original Design A)*, C'_1 (Design B) and C'_2.

The increase in directional stability significantly decreases the size of the broaching plot at the higher speed.

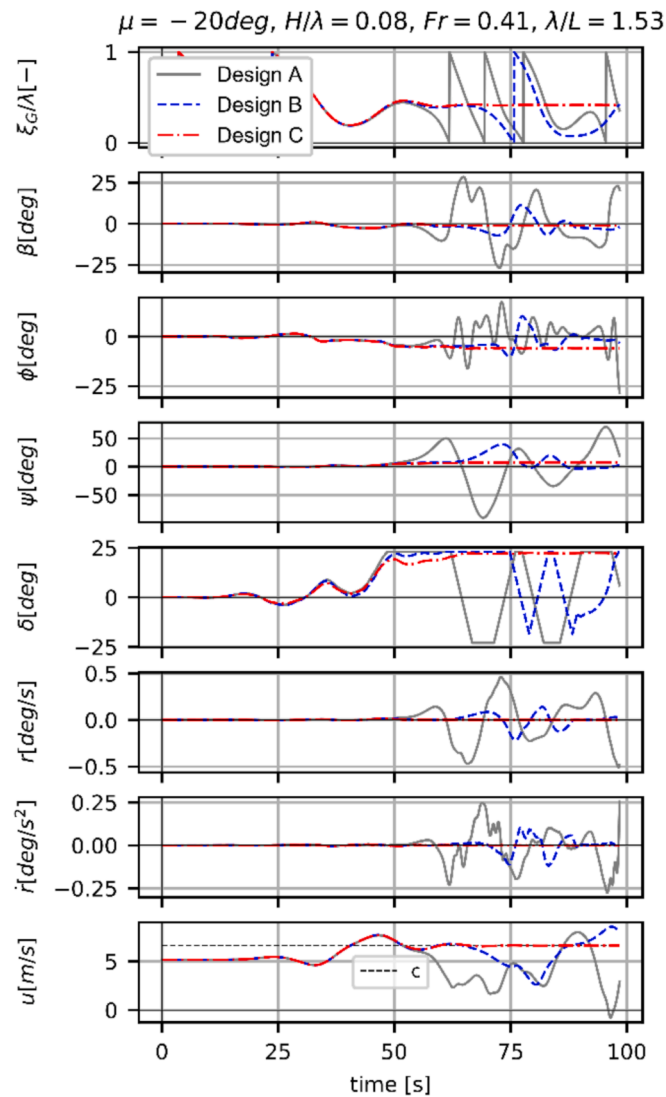The same analysis was carried out for the steering ability. This was

Fig. 20. Comparison of the time histories of a numerical free-sailing run between Design A (original), Design B (increased directional stability) and Design C (enhanced steering ability). The initial vessel forward speed corresponds to Fr = 0.41 and the non-dimensional wave length to 1.53. The other constant simulation parameters are summarised at the top of the picture. Design A shows a rather quick inception of broaching-to, which occurs around 60 s after the start of the simulations. Design B also experiences a broach, but the increase of turning rate and heading deviation is retarded (it occurs 10 s later than the original.

Design A) and the turning acceleration is significantly lower. Design C instead managed to keep it course and surf-rides on the wave, only.

done by increasing the steering force from the waterjets by up to *50%*. The results are shown in Fig. 25.

Increasing the steering force has a different effect compared to the effect of the more directionally stable design. A *50%* increase in the steering force reduces the occurrence of broaching-to at lower speed, whereas broaching still occurs at higher wave length, height and forward speed.

7. Concluding remarks

The forces and moments on a high speed hard-chine craft in waves were measured by means of captive model tests in following and stern-quartering waves at the Seakeeping & Manoeuvring Basin of MARIN, in Wageningen. The results were used to validate the forces and moments
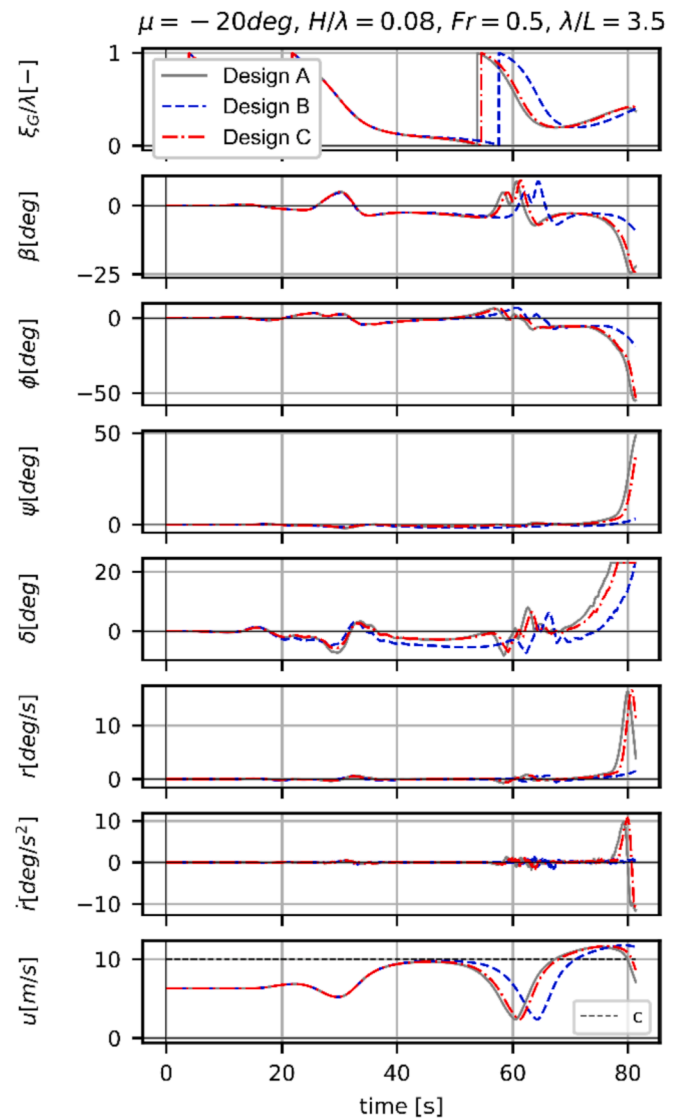
Fig. 21. Comparison of the time histories of a numerical free-sailing run between the Design A (original), Design B (more course stable) and Design C (enhanced steering ability). The initial vessel forward speed corresponds to Fr = 0.5 and the non-dimensional wave length $\lambda/L = 3.5$. The other constant simulation parameters are summarised at the top of the picture. In this case the waves are longer, higher and more powerful. Broaching-to occurs for the design A and C: it is extremely quick, the drift angle β, the roll angle Φ and the yaw turning velocity r reach frightening large values. The Design B instead does not experience the same instability; the vessel is sailing at high-speed thus being more directionally stable. At the very end of the simulation the heading starts to increase but it is retarded with respect to the other two cases and at significantly smaller turning acceleration.

predicted using a 3D time domain blended potential flow BEM (3D BEM) used to simulate the behaviour of the craft in following and stern-quartering seas.

It was shown that this 3D BEM can be used to predict the wave induced Froude-Krylov force. The steering loads are well presented in the simulation program. On the other hand, the predicted forces and moments induced by the sway velocity need to be corrected in order to match the measured results, and a correction method was shown. The other manoeuvring forces, such as those caused by yaw velocity and heel angle are included in the simulations. The yaw velocity induced coefficients are difficult to obtain by means of model tests and further research is required. The effect of the heel-coupling terms on the behaviour of the vessel sailing in the following sea is important;
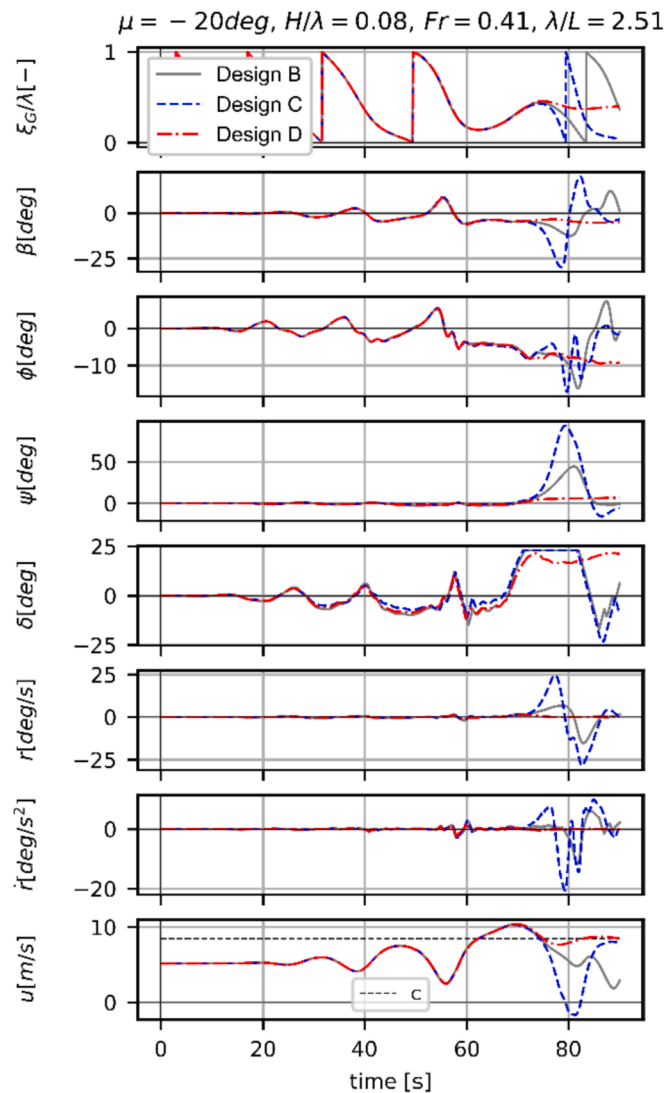
Fig. 22. Comparison of the time histories of a numerical free-sailing run between the Design B (more course stable), Design C (enhanced steering ability) and Design D (both enhanced directional stability and turning effectiveness). The initial vessel forward speed corresponds to $Fr = 0.41$ and the non-dimensional wave length $\lambda/L = 2.51$. The other constant simulation parameters are summarised at the top of the picture. Broaching-to occurs for the designs B and C. The yaw turning rate and yaw turning acceleration of Design B is considerably lower than Design C. Design D is more effective: only a surf-ride occurs.

however, the heel induced loads were considered in the simulations but their effect on the steering qualities of the vessel was not assessed in this work. For details on this topic, the reader can refer to (Bonci et al., 2019; Matsuda and Umeda, 2000; Oltmann, 1993; Hashimoto et al., 2011; Yasukawa and Yoshimura, 2014; Renilson and Tuite, 1995, 1996, 1997).

The manoeuvring terms were implemented into the 3D BEM and their effect on the onset of broaching-to of the SAR NH-1816 craft was investigated. For this particular high-speed craft, the directional stability and turning ability were varied, showing that:

- An increase in directional stability has little effect on the size of the broaching zone below a wavelength to ship length ratio of around *2.5*, however it does reduce the size of the broaching zone for longer waves.
- An increase in the steering ability, as a result of an increase in steering force available, reduces the size of the broaching zone,
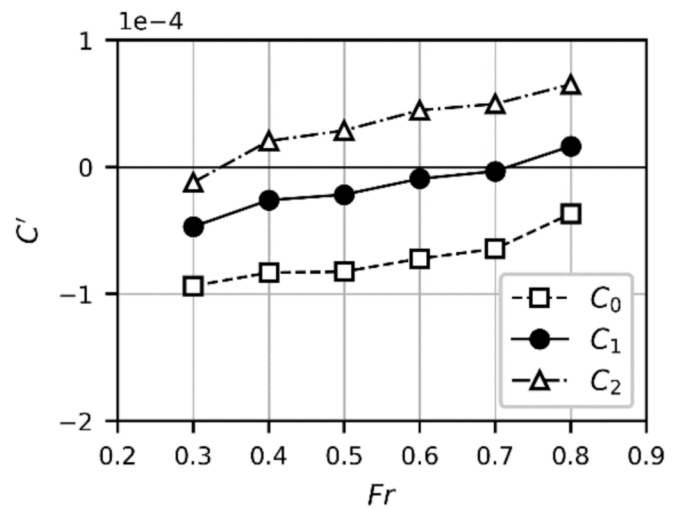

Fig. 23. Comparison of the C-index in calm water as function of the Froude number. The values are obtained by modifying the linear coefficients in sway and yaw towards a more directionally stable hull.

particularly for low speeds and low wavelength to ship length ratios up to *2.5*.

- It was shown that the size of the broaching zone could be reduced compared to the original design by the enhancement of both the directional stability and the steering effectiveness. This is preferable because the modifications of the stern appendages configurations, aimed to improve the ship manoeuvrability, are often limited.

Future research studies must investigate the steering qualities of a fast vessel in realistic, irregular following sea states. This would widen the validity of the findings of this work. Another fundamental aspect not touched by this work is the assessment of the vulnerability of a vessel to dynamic instability events. This is an important and necessary step to judge in absolute sense the quality of a vessel when sailing in following waves. Future developments in that sense are foreseen by IMO and by the research institutions, in collaboration with several fast vessel operators.

List of symbols

|		
$b_{\delta\psi}$	Auto-pilot proportional coefficient	[deg/deg]
$c_{\delta\psi}$	Auto-pilot damping coefficient	[deg/(deg/s)]
c_M	Impeller inflow momentum coefficient	[-]
c	Wave crest celerity	[m/s]
$Fr = U/sqrt$ $(g*L)$	Froude number	[-]
GM_T	Metacentric height	[m]
H	Wave height	[m]
I_x, I_Z	Roll and yaw inertia	[kgm^4]
J_x, J_Z	Roll and yaw added inertia	[kgm^4]
K^*_ϕ, K_v, K_r	Roll manoeuvrability coefficients induced by heel (hydrodynamic), sway and yaw velocities	[Nm, Ns, Nms]
L	Ship reference length	[m]
m	Ship mass	[kg]
m_x, m_y	Ship added mass in surge and yaw	[kg]
N_ϕ, N_v, N_r	Yaw hydrodynamic coefficients induced by heel, sway and yaw velocities	[Nm, Ns, Nms]
Q	Waterjet flow	[m^3/s]
R_T	Total motion resistance	[N]
Y_ϕ, Y_v, Y_r	Sway hydrodynamic coefficients induced by heel static angle, sway and yaw velocities	[N, Ns/m, Ns]
u	Advance speed	[m/s]
v	Sway speed	[m/s]
r	Yaw velocity	[rad/s]
u_{NOZ}	Flow speed at the waterjets nozzle	[m/s]
x_{NOZ}	Longitudinal location of the nozzle with respect to G	[m]
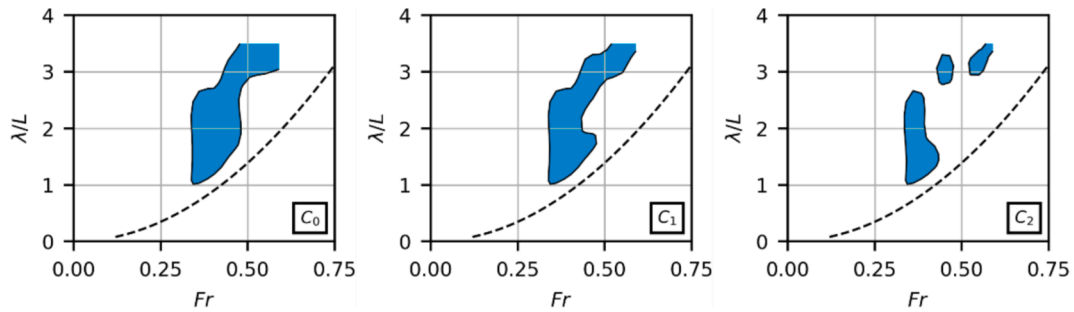
Fig. 24. Three different broaching zone plots obtained by progressively increasing the directional stability of the vessel.
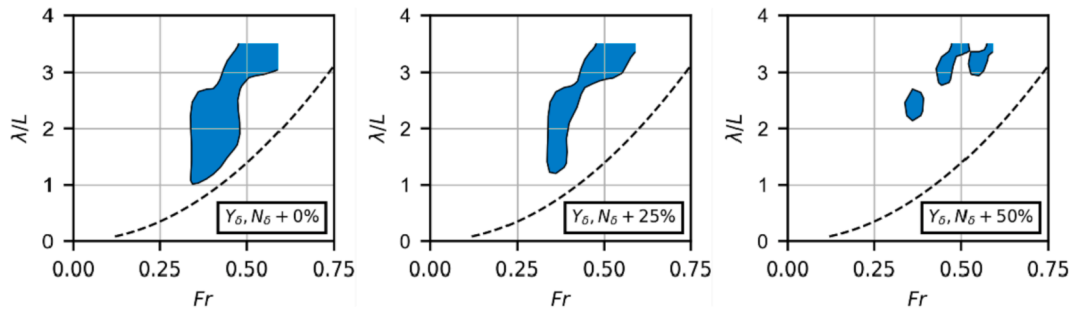

Fig. 25. Three different broaching zone plots obtained by progressively increasing the steering effectiveness of the waterjets.

(*continued*)

z_{NOZ}	Vertical location of the nozzle with respect to G	[m]
α_x	Longitudinal centre of the distribution of sway added mass	[m]
β	Drift angle	[deg]
δ	Steering angle	[deg]
Φ, θ, ψ	Roll, pitch, yaw angle	[deg]
μ	Wave incidence angle	[deg]
ξ_G	Longitudinal location of the ship centre of gravity G in the wave	[m]
λ	Wave length	[m]

Declaration of competing interest

The authors declare that they have no known competing financial interests or personal relationships that could have appeared to influence the work reported in this paper.

Appendix

This Appendix contains the comparison between the measured and predicted captive tests results. The numerical captive tests were carried out over a number of conditions different than the cases tested in the experiments. This is aimed to highlight a trend of the manoeuvring forces and moments on a wider domain of ship speed and wave combinations investigated in the simulations. A summary of the conditions investigated is reported in Table T.1.

Table T.1
Summary of the conditions of the numerical captive model tests. For each of the 7 Froude number, 4 wave length were simulated. The wave steepness H/λ, the wave incidence angles μ and the drift angles β are the same tested in the experimental campaign (see Tables 3 and 4).

Fr	λ/L	H/λ	β and μ[deg]
0.32	0.75, 1, 1.25,1.75	0.06	$\beta = 0, 5, 10$
0.38	1, 1.25, 1.5, 2		$\mu = 0, 5, 10$
0.43	1.25, 1.5, 1.75, 2.25		
0.48	1.5, 1.75, 2, 2.5		
0.53	2.0, 2.25, 2.5, 3		
0.575	2.25, 2.5, 2.75, 3.25		
0.59	2.5, 2.75, 3, 3.5		

The figures included in this Appendix show the comparison between measurements and prediction of the following quantities: the amplitude a, the phase φ, the mean value η, of the wave surging force X'_W (Fig. A.1 and A2), of the sway velocity induced coefficients Y'_v, K'_v and N'_v (Fig. A.3 and A.4), and of the wave coefficients Y'_μ, K'_μ and N'_μ (Fig. A.5 and A.6); these terms are depicted alternatively as functions of Froude number *Fr* and non-

dimensional wave length λ/L. The wave surging force and the wave coefficients computed by the 3D BEM were not corrected; instead the numerical sway velocity induced coefficients were corrected keeping into account the empirical results. The wave surging force terms reported in the plots refer to a zero wave incidence angle ($\mu = 0$). The measurements are denoted with white squares; the numerical prediction with black dots.
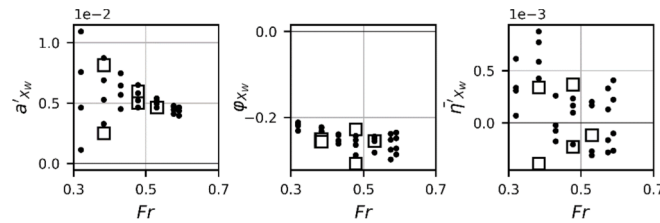

Fig. A.1. Comparison of the measured (white squares) and predicted (black dots) captive tests results for the wave surging force X'_W. In the columns, starting from the left: amplitude, phase and mean values of the sinusoidal signal function of the location in the wave ξ_G/λ. The terms are plotted as function of Froude number Fr.
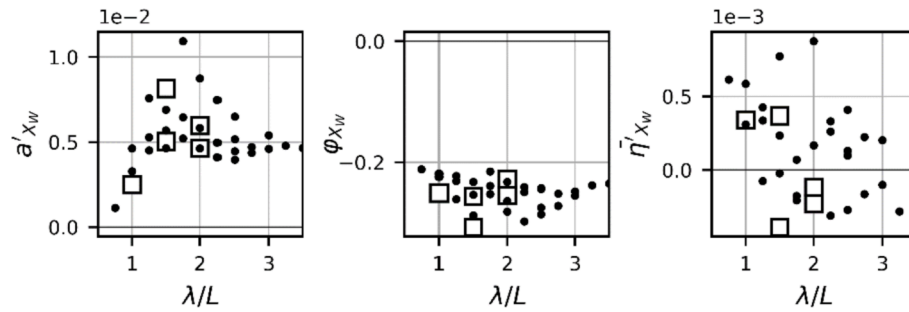

Fig. A.2. Comparison of the measured (white squares) and predicted (black dots) captive tests results for the wave surging force X'_W. In the columns, starting from the left: amplitude, phase and mean values of the sinusoidal signal function of the location in the wave ξ_G/λ. The terms are plotted as function of the non-dimensional wave length λ/L.
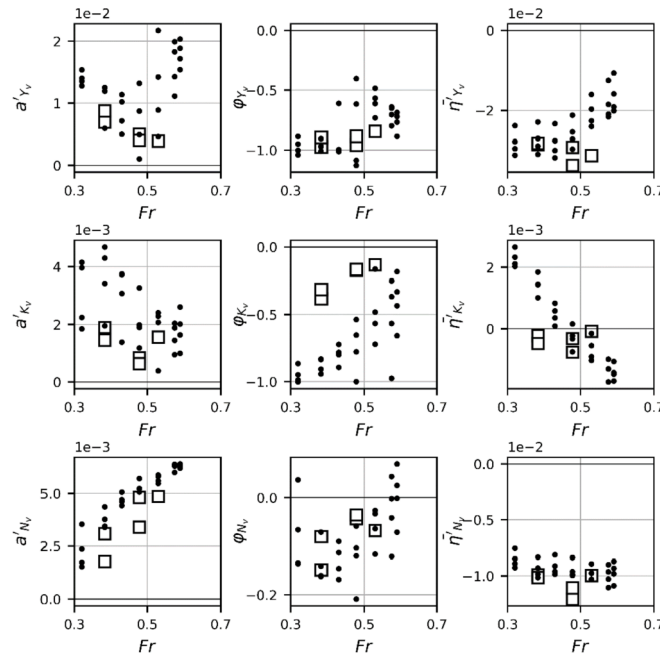

Fig. A.3. Comparison of the measured (white squares) and predicted (black dots) captive tests results for the sway velocity induced coefficients. In the rows, starting from the top: Y'_v, K'_v and N'_v; in the columns, starting from the left: amplitude, phase and mean values of the sinusoidal signal function of the location in the wave ξ_G/λ. The terms are plotted as function of Froude number Fr.
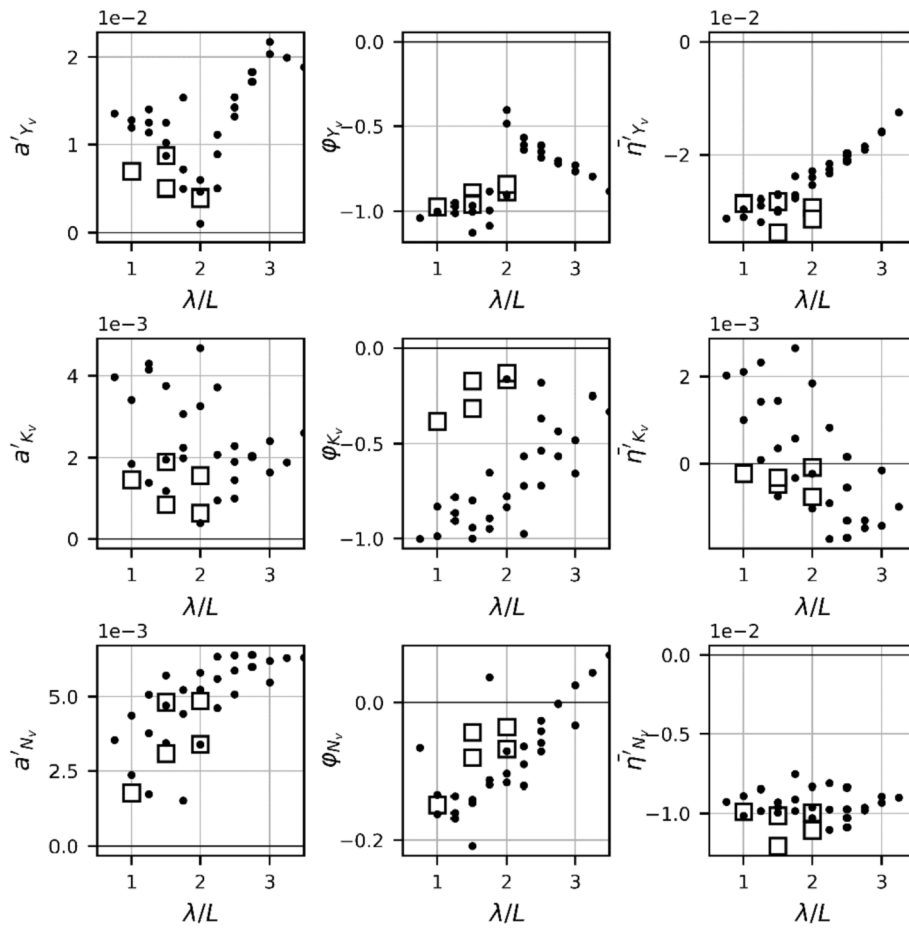
Fig. A.4. Comparison of the measured (white squares) and predicted (black dots) captive tests results for the sway velocity induced coefficients. In the rows, starting from the top: Y'$_v$, K'$_v$ and N'$_v$; in the columns, starting from the left: amplitude, phase and mean values of the sinusoidal signal function of the location in the wave ξ_G/λ. The terms are plotted as function of the non-dimensional wave length λ/L.

Fig. A.5. Comparison of the measured (white squares) and predicted (black dots) captive tests results for the wave incidence angle induced coefficients. In the rows, starting from the top: Y'$_\mu$, K'$_\mu$ and N'$_\mu$; in the columns, starting from the left: amplitude, phase and mean values of the sinusoidal signal function of the location in the wave ξ_G/λ. The terms are plotted as function of Froude number Fr.
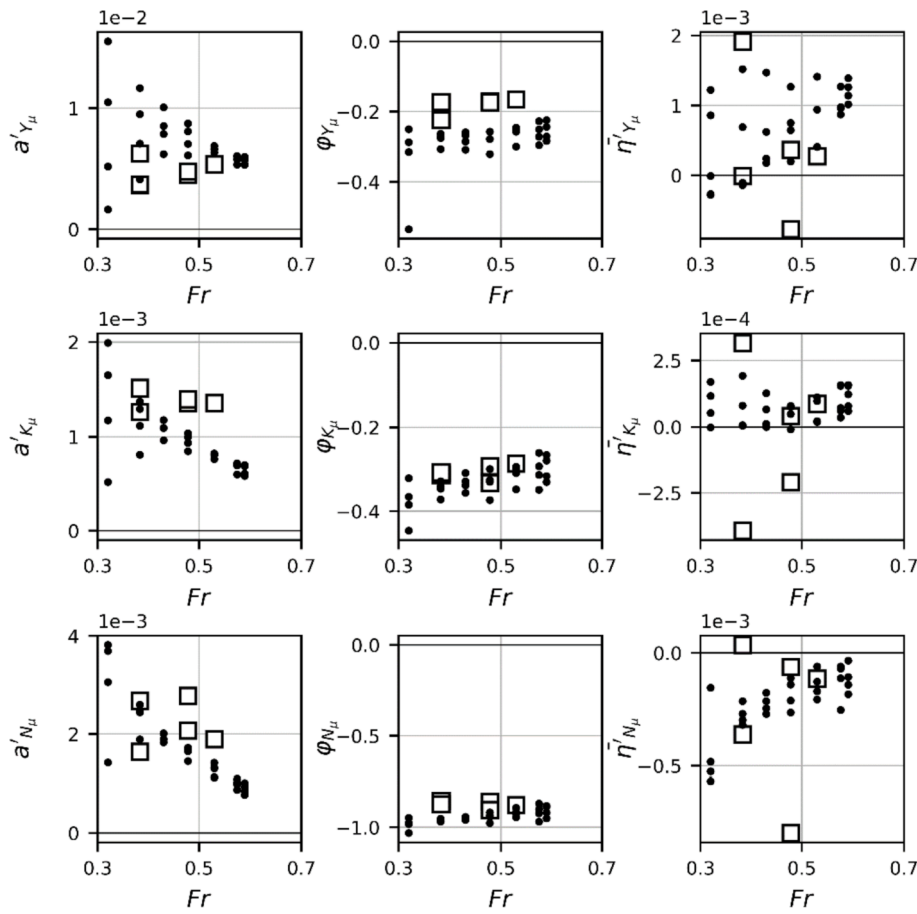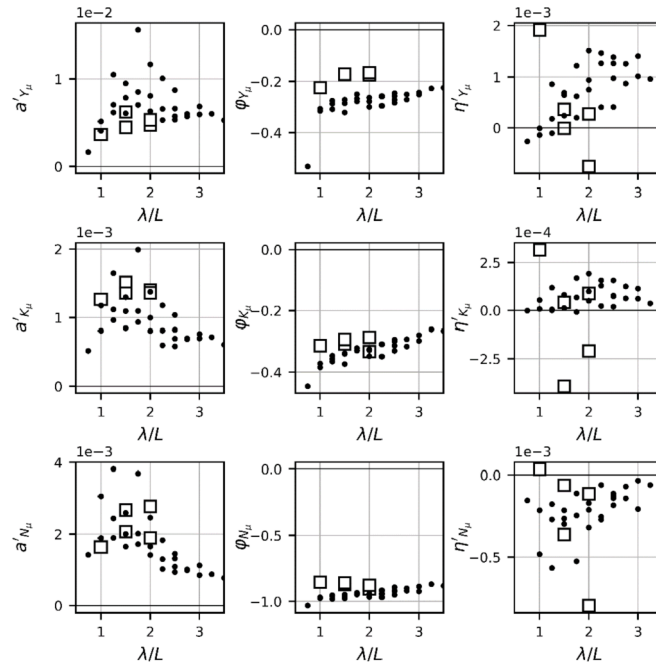

Fig. A.6. Comparison of the measured (white squares) and predicted (black dots) captive tests results for the wave incidence angle induced coefficients. In the rows, starting from the top: Y'$_\mu$, K'$_\mu$ and N'$_\mu$; in the columns, starting from the left: amplitude, phase and mean values of the sinusoidal signal function of the location in the wave ξ_G/λ. The terms are plotted as functions of the non-dimensional wave length λ/L.

References

Bailey, P.A., Price, W., Temarel, P., 1997. A unified mathematical model describing the maneuvering of a ship travelling in a seaway. Trans. R. Inst. Nav. Archit. 140, 131–149.

Bonci, M., Renilson, M.R., Jong, P., Walree, F., Keuning, A.J., Huijsmans, R.H.M., 2017. Experimental and Numerical Investigation on the Heel and Drift Induced Hydrodynamic Loads of a High-Speed Vessel, 14th Conference on Fast Sea Transportation. Nantes (France).

Bonci, M., Renilson, M.R., Jong, P., Walree, F., Keuning, A.J., Huijsmans, R.H.M., 2018. The heel-sway-yaw coupling on a high-speed craft in calm water, the Transaction of the Royal Institution of Naval Architects. Part B - Int. J. High-Speed Craft Technol. 160, 121–129.

Bonci, M., De Jong, P., Van Walree, F., Renilson, M., Keuning, A.J., Van't Veer, R., 2019. The heel-induced sway force and yaw moment of a high-speed craft in following regular waves. J. Mar. Sci. Technol. https://doi.org/10.1007/s00773-019-00637-0.

Du Cane, P., Goodrich, G., 1962. The following sea, broaching and surging. Trans. RINA 104.

Cohen, S.H., Blount, D.L., 1986. Research plan for the investigation of dynamic instability of small high-speed craft. SNAME Transactions 94, 197–214.

Coleman, H.W., Steele, W.G., 1999. Experimentation and Uncertainty Analysis for Engineers, second ed. Wiley, New York.

Conolly, J.E., 1972. Stab. control in Waves: a Surv. Probl. 14, 186–193.

Fossen, T., 2003. A nonlinear unified state-space model for ship maneuvering and control in a seaway. J. Bifurc. Chaos 15, 2717–2746.

Hashimoto, H., Umeda, N., Matsuda, A., 2004. Importance of several nonlinear factors on broaching prediction. J. Mar. Sci. Technol. 9, 80–93.

Hashimoto, H., Umeda, N., Matsuda, A., 2011. Model Experiment on Heel-Induced Hydrodynamic Forces in Waves for Realising Quantitative Prediction of Broaching, Contemporary Ideas on Ship Stability and Capsizing in Waves.

ITTC, 2014. Uncertainty Analysis for Manoeuvring Predictions Based on Captive Manoeuvring Tests. ITTC. Recommended procedure no. 7.5-02-06.04.

De Jong, P., 2011. Seakeeping Behaviour of High-Speed Ships - an Experimental and Numerical Study. Ph.D. dissertation. Technical University of Delft.

De Jong, P., Van Walree, F., 2008. Hydrodynamic Lift in a Time-Domain Panel Method for the Seakeeping on High Speed Ships, 6th International Conference on High-Performance Marine Vehicles. Naples (Italy).

De Jong, P., Van Walree, F., 2009. The development and validation of a time-domain panel method for the seakeeping of high-speed ships. In: 10th International Conference on Fast Sea Transportation. Athens (Greece).

De Jong, P., Van Walree, F., Renilson, M.R., 2013. The Broaching of a Fast Rescue Craft in Following Seas, 12th International Conference on Fast Sea Transportation. Amsterdam (The Netherlands).

De Jong, P., Renilson, M., Walree, F., 2015. The Effect of Ship Speed, Heading Angle and Wave Steepness on the Likelihood of Broaching-To in Astern Quartering Seas, 12th International Conference on the Stability of Ships and Ocean Vehicles. Glasgow (United Kingdom).

Keuning, A.J., 2006. Grinding the bow. Int. Shipbuild. Prog. 53, 281–310.

Keuning, A.J., Visch, G.L., Gelling, J.L., De Vries Lentsch, W., Burema, G., 2011. Development of a new SAR boat for the royal Netherlands Sea Rescue institution. In: Proceedings of the 11th International Conference on Fast Sea Transportation (FAST2011). Hawaii (USA).

Maki, A., Umeda, N., Renilson, M.R., 2010. Analytical formulae for predicting the surf-riding threshold for a ship in following Seas. J. Mar. Sci. Technol. 15, 218–229.

Matsuda, A., Umeda, N., 2000. New Experimental Procedure for Identifying Manoeuvring Coefficients of a Ship Suffering Broaching in Following and Quartering Seas, Fourth Osaka Colloquium on Seakeeping Performance of Ships.

Nicholson, K., 1974. Some Parametric Model Experiments to Investigate Broaching-To, International Symposium on the Dynamics of Marine Vehicles and Structures in Waves.

Oltmann, P., 1993. Roll - an often neglected element of manoeuvring, MARSIM 93. In: International Conference on Marine Simulation and Ship Manoeuvrability, vol 2. St. John's, Newfoundland (Canada).

Principles of Naval Architecture, Vol III - Seakeeping and Manoeuvrability, 1988. Edward V. Lewis, The Society of Naval Architects and Marine Engineers.

Reed, A., Beck, R., 2018. Mathematical Models of Maneuvering in Waves: Historical Perspectives and the State of the Art, 13th International Conference on the Stability of Ships and Ocean Vehicles (STAB2018). Kobe (Japan).

Renilson, M.R., 1981. The Broaching of Ships in Following Seas. Ph.D. dissertation. University of Glasgow.

Renilson, M.R., 2014. Behaviour of High-Speed Craft in Following Sea, 10th Symposium on High Speed Marine Vehicles, Naples (Italy).

Renilson, M.R., Driscoll, A., 1982. Broaching - an investigation into the loss of directional control in severe following seas. Transactions RINA 124, 253–273.

Renilson, M., Tuite, A., 1995. The Effect of GM on Manoeuvring of High Speed Container Ship. 11th International Maritime and Shipping Symposium: 21st Century Shipping.

Renilson, M., Tuite, A., 1996. The Effect of GM and Loss of Control of a Planing Mono-Hull in Following Seas, High Speed Marine Craft, Safe Design and Safe Operation.

Renilson, M., Tuite, A., 1997. The effect of GM on broaching and capsizing of small fishing vessels in following seas. STAB97. In: Proceedings of the 6th International Conference on Stability of Ships and Ocean Vehicles, pp. 149–161. Varna (Bulgaria).

Renilson, M.R., Tuite, A., 1998. Broaching-to: A Proposed Definition and Analysis Method, 25th American Towing Tank Conference. Iowa (USA).

Resolution, I.M.O., 2002. MS vol 137, 76, Standards for Ship Manoeuvrability.

Skejic, R., Faltinsen, O.M., 2008. A unified seakeeping and maneuvering analysis of ships in regular waves. J. Mar. Sci. Technol. 13, 371–394.

Spyrou, K.J., 1996. Dynamic instability in quartering seas: the behavior of a ship during broaching. J. Ship Res. 40, 46–59.

Spyrou, K.J., 2006. Asymmetric surging of ships in following seas and its repercussions for safety. Nonlinear Dyn. 43, 149–172.

Umeda, N., 1999. Nonlinear dynamics of ship capsizing due to broaching in following and stern-quartering seas. J. Mar. Sci. Technol. 4, 16–26.

Umeda, N., Hamamoto, M., 2000. Capsize of ship models in following/quartering waves: physical experiments and nonlinear dynamics. Philos. Trans. R. Soc. London, Ser. A: Math. Phys. Eng. Sci. 358.

Umeda, N., Matsuda, A., 2000. Broaching in Following and Quartering Seas - Theoretical Attempts and New Prevention Device, 7th International Conference on the Stability of Ships and Marine Vehicles, pp. 460–470. A.

Umeda, N., Yamamura, S., Matsuda, A., Maki, A., Hashimoto, H., 2008. Model experiments on extreme motions of a wave-piercing tumblehome vessel in following and quartering waves. J. Jpn. Soc. Nav. Archit. Ocean Eng. 8, 123–129.

Umeda, N., Usada, S., Mizumoto, K., Matsuda, A., 2016. Broaching probability for a ship in irregular stern-quartering waves: theoretical prediction and experimental validation. J. Mar. Sci. Technol. 21, 23–37.

Van Walree, F., 1999. Computational Methods for Hydrofoil Craft in Steady and Unsteady Flow. Ph.D. dissertation. Technical University of Delft.

Van Walree, F., De Jong, P., 2011. Validation of a Time Domain Panel Code for High Speed Craft Operating in Stern and Quartering Seas, 11th International Conference on Fast Sea Transportation. Honolulu (Hawaii).

Yasukawa, H., Yoshimura, Y., 2014. Roll-coupling effect on ship maneuverability. Ship Technol. Res. 61, 16–32.

Yasukawa, H., Hirata, N., Nakayama, Y., 2016. High-speed ship maneuverability. J. Ship Res. 60, 239–258.